Science of the Total Environment xxx (2016) xxx–xxx

Contents lists available at ScienceDirect

Science of the Total Environment

journal homepage: www.elsevier.com/locate/scitotenv

Future hydrological regimes and glacier cover in the Everest region: The case study of the upper Dudh Koshi basin

Andrea Soncini [a], Daniele Bocchiola [a,b,*], Gabriele Confortola [a], Umberto Minora [a], Elisa Vuillermoz [b], Franco Salerno [b,c], Gaetano Viviano [b,c], Dibas Shrestha [d], Antonella Senese [e], Claudio Smiraglia [e], Guglielmina Diolaiuti [b,e]

[a] Politecnico di Milano, Dept. Civil and Environmental Eng., L. da Vinci 32, 20133 Milano, Italy
[b] EVK2CNR Committee, Via San Bernardino 145, 24126 Bergamo, Italy
[c] Water Research Institute, National Research Council (IRSA—CNR), Via del Mulino 19, Brugherio, MB 20861, Italy
[d] Nepal Academy of Science and Technology, NAST, Kathmandu, Nepal
[e] University Milano, Dept. Earth Sciences, Mangiagalli 34, 20133 Milano, Italy

HIGHLIGHTS

- We pursued glacio-hydrological modeling of the Dudh Koshi river of Nepal.
- We used *in situ* data gathered during 2012–2014, historical ground and satellite data.
- We investigated the impact of climate change until 2100 using IPCC AR5 scenarios.
- Stream flows will be largely reduced (−30% or so) until 2100.
- Ice volume in the catchment will largely decrease (−50% or so) until 2100.

GRAPHICAL ABSTRACT

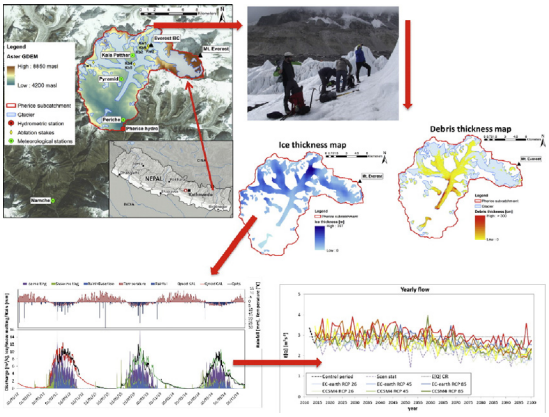

ARTICLE INFO

Article history:
Received 5 March 2016
Received in revised form 12 April 2016
Accepted 19 May 2016
Available online xxxx

Editor: D. Barcelo

Keywords:
Himalayan water towers
Climate change
Glaciers' evolution
Hydrological projections

ABSTRACT

Assessment of future water resources under climate change is required in the Himalayas, where hydrological cycle is poorly studied and little understood. This study focuses on the upper Dudh Koshi river of Nepal (151 km^2, 4200–8848 m a.s.l.) at the toe of Mt. Everest, nesting the debris covered Khumbu, and Khangri Nup glaciers (62 km^2). New data gathered during three years of field campaigns (2012–2014) were used to set up a glacio-hydrological model describing stream flows, snow and ice melt, ice cover thickness and glaciers' flow dynamics. The model was validated, and used to assess changes of the hydrological cycle until 2100. Climate projections are used from three Global Climate Models used in the recent IPCC AR5 under RCP2.6, RCP4.5 and RCP8.5. Flow statistics are estimated for two reference decades 2045–2054, and 2090–2099, and compared against control run CR, 2012–2014. During CR we found a contribution of ice melt to stream flows of 55% yearly, with snow melt contributing for 19%. Future flows are predicted to increase in monsoon season, but to decrease yearly (−4% *vs* CR on average) at 2045–2054. At the end of century large reduction would occur in all seasons, *i.e.* −26% *vs* CR on average at 2090–2099. At half century yearly contribution of ice melt would be on average 45%, and snow melt

* Corresponding author at: Politecnico di Milano, Dept. Civil and Environmental Eng., L. da Vinci 32, 20133 Milano, Italy.
E-mail address: daniele.bocchiola@polimi.it (D. Bocchiola).

http://dx.doi.org/10.1016/j.scitotenv.2016.05.138

28%. At the end of century ice melt would be 31%, and snow contribution 39%. Glaciers in the area are projected to thin largely up to 6500 m a.s.l. until 2100, reducing their volume by −50% or more, and their ice covered area by −30% or more. According to our results, in the future water resources in the upper Dudh Koshi would decrease, and depend largely upon snow melt and rainfall, so that adaptation measures to modified water availability will be required.

1. Introduction

Evidence of global change as set out by the fifth assessment report of the International Panel on Climate Change (AR5 IPCC, 2013) indicates a large expected impact on the highest altitude areas. Several studies recently displayed that future snow and ice cover worldwide is projected to shrink down, and that water resources will likely be modified (Meybeck et al., 2001; Barnett et al., 2005; Hagg and Braun, 2005; Bocchiola et al., 2010; Immerzeel et al., 2010; Bocchiola et al., 2011; Soncini et al., 2015; Migliavacca et al., 2015). Several countries worldwide depend upon water supplied by mountains, and climate change may lead to extinction of permanently cryospheric areas, and decrease of the available water (Barnett et al., 2005; Viviroli et al., 2007; Bolch et al., 2011, 2012; Kääb et al., 2012; Diolaiuti et al., 2012a, 2012b). Water and food security for downstream populations are therefore at stake (*e.g.* Aase et al., 2009; Groppelli et al., 2011a; Viganò et al., 2015). Climate change in the mountain areas changes water distribution in space and time (*e.g.* Rohrer et al., 1994; Beniston, 1997; Laternser and Schneebeli, 2003), including the frequency of extreme floods, and droughts (*e.g.* Liu et al., 2003; Bocchiola et al., 2011; Groppelli et al., 2011a; Confortola et al., 2013; Bocchiola, 2014), further increasing natural hazards.

The mountain range of the Hindu Kush, Karakorum and Himalaya (HKKH) contains a large amount of glacier ice, and in the last fifty years it underwent climate change and subsequent ice cover shrinking (*e.g.* Berthier et al., 2007; Salerno et al., 2008; Kehrwald et al., 2008; Benn et al., 2012; Gardelle et al., 2012; Bocchiola and Diolaiuti, 2013; Minora et al., 2013; Thakuri et al., 2014; Salerno et al., 2015). In Nepal, subsistence agriculture practiced by 90% of the active population is highly water dependent (Brown and Shrestha, 2000; Palazzoli et al., 2015), and there is an upwelling need of tools for water resources management to effectively sustain agricultural politics (Chalise et al., 2003; Rees et al., 2006), and to adapt water allocation strategies against climate change (Aggarwal et al., 2004; Palazzoli et al., 2105). Moreover, use of water for small hydropower plants, *albeit* low in percentage (about 3% of total energy production) is increasing (Sharma, 1996; Pokharel, 2007), and may be impacted by forthcoming water shortage. Long term field measurements in the highest glacierized areas are seldom available (see Chalise et al., 2003; Konz et al., 2007; Rowan et al., 2015), and assessment of hydro-climatic trends is possible only at relatively low altitudes (*e.g.* Salerno et al., 2015).

Here, we investigated recent and prospective glacio-hydrological dynamics of the upper part of the Dudh Koshi (milk river) basin of Nepal, at the toe of Mt. Everest, taking input of snow and ice melt from the Khumbu, and Khangri Nup glaciers. These glaciers have experienced a negative mass balance in the last three decades (*e.g.* Bolch et al., 2011; Thakuri et al., 2014), and accordingly investigation of their prospective dynamics is warranted (see *e.g.* Shea et al., 2015). We could build here on data from recent field campaigns, that provided new updated data of glacial dynamics of the Khumbu and Khangri Nup glaciers. These new data include i) hydrological fluxes at a flow station operating during 2012–2014 at Pheriche (4200 m a.s.l.), ii) stake based ice melt (bare and debris covered ice, 5050–5250 m a.s.l.), measured during 2012–2014, iii) newly estimated debris cover thickness based on *in situ* measurements, and satellite investigation, iv) ice flow velocity from ice stakes, and v) snow melt modeling using recent snow depth, and fresh snow depth and density data.

Based on such data we pursued a modeling exercise based on several tools, namely i) a semi-distributed hydrological model, ii) a distributed melt model for buried and clean ice, iii) a simple ice flow model to avoid inconsistent "static" glacier cover, iv) a snow melt model, and v) climate projections until 2100, based upon (properly downscaled) outputs from three Global Circulation Models (GCMs) under three representative concentration pathways (RCP) scenarios.

The present results come from activities carried out within the SHARE-Paprika project (2010−2013), and the Khumbu Hydrology project (2014–2015), funded by the EVK2CNR committee of Italy. The manuscript is organized as follows. In Section "Region of investigation" we describe the upper Dudh Koshi river, and climate therein. In Sections "Database and Methods" we describe the data base, including historical weather data, and newly gathered hydrological and glaciological data, and we report our methodology. In Section "Results" we provide the outputs of our modeling effort, and accuracy of the findings. In the Section "Discussion" we benchmark our results against available studies in the literature, we deepen into the expected behavior of the upper Dudh Koshi catchment as per our climate projections, and we highlight limitations of the study, and outlooks. We then draw some conclusions, and outline possible future efforts.

2. Region of investigation

The Dudh Koshi basin (closed at Pheriche, 27.88° N, 86.82° E, Fig. 1) is located on the southern slopes of Mt. Everest (eastern part of central Himalaya), extending from an elevation of 4200 to 8848 m a.s.l. The basin is part of the Sagarmatha (Everest) National Park (SNP), along the Khumbu Valley. SNP is the world's highest protected area, visited every year by plenty of tourists (over 30,000 in 2008), including climbers to Everest and other summits (Tartari et al., 2008; Amatya et al., 2010; Salerno et al., 2013). The two glaciers (Khumbu, and Khangri Nup) laid in the study catchment (151 km^2) occupy 62 km^2, *i.e.* 41% of the basin. Both glaciers are debris covered (37% and 24% of the total glacier surface, respectively), with their ablation zone almost entirely covered by debris (Thakuri et al., 2014). These glaciers are identified as temperate summer-accumulation type, fed mainly by summer precipitation from the South Asian monsoon system (*e.g.* Yao et al., 2012; Thakuri et al., 2014). Recently, Thakuri et al. (2014) traced the surface area loss of glaciers in SNP since the early 1960s. The area shrinkage of Khumbu and Khangri glaciers estimated therein is low compared to that of other glaciers in the Himalayan region (−6.5%, and −7.5%, respectively, with the sign minus indicating a percentage decrease with respect to the initial values, used here and in the following). However, the Snow Line (SL) shifted of *ca.* +327 m (from 5403 m a.s.l. to 5730 m a.s.l.) and +232 m (from 5352 m to 5584 m a.s.l.), respectively. This suggests that these glaciers have experienced a consistent negative mass balance and down wasting, as commonly happening for debris covered glacier (*e.g.* Bolch et al., 2011). Bolch et al. (2011) assessed mass balance of Khumbu and Khangri glaciers, and reported that specific mass loss for 1970–2007 was nearby −0.28 and −0.27 m w.e. $year^{-1}$, respectively, with a lowering of debris surface of the Khumbu glacier of *ca.* −0.38 m $year^{-1}$ during the same period. The mass loss of these two glaciers is similar to the

Please cite this article as: Soncini, A., et al., Future hydrological regimes and glacier cover in the Everest region: The case study of the upper Dudh Koshi basin, Sci Total Environ (2016), http://dx.doi.org/10.1016/j.scitotenv.2016.05.138

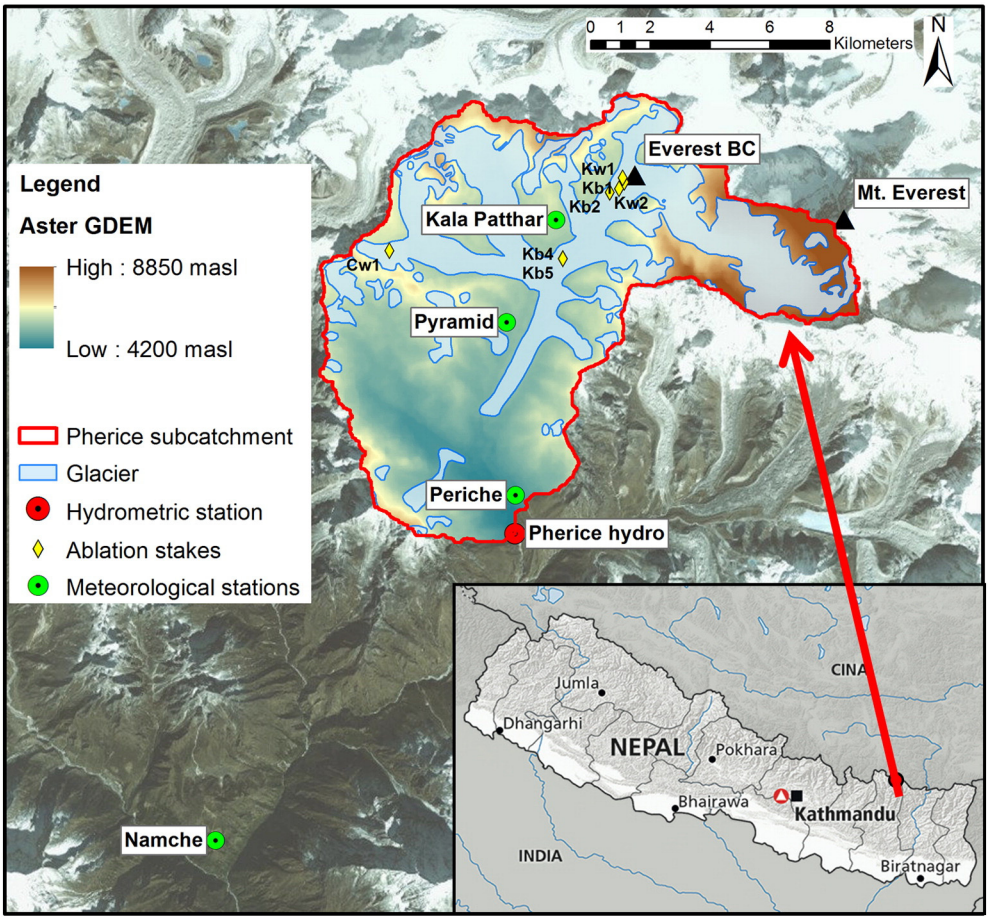

Fig. 1. Region of investigation: Dudh Koshi basin closed at Pheriche, Sagarmatha National Park, Nepal. The hydro-meteorological stations are reported as well as the seasonal (May–October 2014) ablation stakes (see Table 1). Kw, Khumbu clean ice stakes. Cw, Khangri Nup clean ice stakes. Kb, Khumbu buried ice stakes.

average mass loss of the 30 reference glaciers worldwide for 1976–2005 (−0.32 m w.e. year^{-1}, Zemp et al., 2009).

The climate zone is Polar Tundra (ET, Peel et al., 2007), with dry and cold winters, warm summers, and mainly monsoonal precipitation. In summer, monsoonal air from the Bay of Bengal generates rainfall as it is forced towards the orographic barrier posed by the Himalayas range. In the study area, four seasons can be identified related to the precipitation (*e.g.* Hannah et al., 2005; Immerzeel et al., 2014). The pre-monsoon season (March to May) displays dry weather, relatively high temperatures and limited cloud cover. The monsoon generally onsets in June, and rainfall is observed almost every day. Around 90% of annual rainfall occurs during June to September (Salerno et al., 2015). In the post-monsoon season (October to November) rainfall activity is substantially reduced. Winter (December to February) is generally dry, with occasional precipitation related to the western circulation (Bookhagen and Burbank, 2006, 2010). The annual total precipitation measured at the Pyramid station (5035 m a.s.l.) is on average 446 mm, with a mean annual temperature of −2.45 °C (Salerno et al., 2015). The flow regime of Himalayan rivers is strictly connected with the Indian summer monsoon, and the Dudh Koshi river is no exception (Savéan et al., 2015). Discharge peaks during the summer monsoon, and large share of summer discharge is expected to derive from ice and snow melt. After the monsoon, river flow slowly decreases, with melting still occurring, and least flows are observed during winter. In spring, before monsoon the rising limb of the hydrograph onsets, as snow melt, and to a lesser extent ice melt start.

3. Database

3.1. Topographic, meteorological and hydrometric data

The ASTER GDEM, Vers. 2 tiles for the Mt. Everest region was used as topographic layer (http://gdem.ersdac.jspacesystems.or.jp). This has vertical and horizontal accuracy of ~20 m and ~30 m, respectively (http://www.jspacesystems.or.jp/ersdac/GDEM/E/4.html), as reported in recent studies covering the area of Himalayas (Li et al., 2012; Tadono et al., 2012; Mukherjee et al., 2013).

Meteorological information was gathered from 4 automatic weather stations (AWSs, Table 1), providing temperature, precipitation, solar radiation, and snow height. These AWSs are property of EVK2CNR committee, and operate since 2003. Snow depth measurements were gathered at Pyramid site during 2003–2014. Measured water level of the Dudh Koshi closed at Pheriche is available during 2012–2014, from a hydrometric station owned by the Italian research institute IRSA-CNR. Flow discharges are calculated using a stage-discharge curve developed in 2014, using flow tracker, and salt tracers. We used daily data, suitable for our modeling approach.

3.2. Field data

We used ice melt measurements (summer 2014) from a network of 13 stakes (6 on Khangri Nup, of which 3 debris free, 7 on Khumbu, 2 debris free), of which seven were usable (1 on Khangri Nup, debris free, 6

Please cite this article as: Soncini, A., et al., Future hydrological regimes and glacier cover in the Everest region: The case study of the upper Dudh Koshi basin, Sci Total Environ (2016), http://dx.doi.org/10.1016/j.scitotenv.2016.05.138

Table 1
Available data base. T is temperature, P precipitation, HS snow height, S solar radiation, L is water level, M_i is ice melt, V_i is ice flow velocity, D_d is debris thickness, ρ_n is fresh snow density, ρ_s is snowpack density.

Station	Alt (m a.s.l.)	Lat (°N)	Lon (°E)	Variable	Resolution used	Period
Namche Bazar	3570	27.80	86.71	T, P	Daily	2003–2014
Pheriche	4258	27.89	86.82	T, P	Daily	2003–2014
Pyramid	5050	27.96	86.81	T, P, S, HS	Daily	2003–2014
Kala Patthar	5600	27.99	86.83	T, P	Daily	2003–2014
Pheriche	4200	27.88	86.82	L	Daily	2012–2014
7 stakes	5050–5240	–	–	M_i, V_i	Various	Spring–Fall 2014
64 points	4900–5300	–	–	D_d	One measure	May 2014
7 cores	5050–5300	–	–	ρ_s	One measure	May 2014
Pyramid		27.96	86.81	ρ_n	At snowfall	May–June 2014

on Khumbu, 2 debris free). These stakes were installed and monitored during spring to fall, 2014. Ice drilling was performed using a Heucke steam drill, normally down to 6–10 m, also depending on functioning of the drill, difficult given low oxygen content of the air. We could rely on data from 4 stakes on debris covered ice, with ablation measured for 12 periods (depending on measurement dates). At the stakes, debris thickness changed during the sampling, so at each survey D_d was measured and taken into account. Debris thickness was sampled in some points during May 2014 on the Khumbu glacier ablation tongue (Approx. from Gorak Shep to Lobuche, Fig. 1). Knowledge of debris thickness is extremely important to model buried ice melt, but few other surveys of debris thickness were performed in the Everest area, due to the labor-intensive nature of this work (*e.g.* Kayastha et al., 2000; Rounce and McKinney, 2014). For three sites with ice covered stakes on the Khumbu glacier, we performed random samplings in a circular area of 30 m radius surrounding our ice stakes (kb1, kb2, kb4 and kb5 together). The sample circles were divided into 4 zones equally spaced, and for each zone 5 samples were taken randomly. The final thickness is the average value from these samples. A second dataset comprises point wise sampled thicknesses nearby 4 stakes (kb3, cb3, cb4, cb5d). Although less representative, these data were necessary to enlarge the sample used to build debris thickness maps from satellite. We could gather 64 measurements of debris thickness. Debris free ablation was available for three stakes, and six different periods, depending upon sampling dates. Measurements of snow density, both fresh and consolidated were also performed. These data were collected in a field survey in May 2014, at two locations along Khumbu valley, *i.e.*, on the Khangri Nup glacier and at Pyramid station. A snow pit 1.70 m deep was dug on the Khangri Nup glacier, at 5613 m a.s.l. Snow cores were taken every 15 cm to estimate snow water equivalent SWE. Six snow samples were taken by vertical coring on Khangri Nup, to estimate snow depth and density (*e.g.* Bocchiola and Rosso, 2007). Khangri Nup glacier is possibly the only reachable area where snow is present at the time of spring surveys (*i.e.* April–May). Fresh snow density was measured at Pyramid AWS in May–June 2014, to estimate new snow water equivalent SWE_n therein. Pyramid site is the only one where snow depth is continuously measured, so we investigated therein snow dynamics (depth, and density, freshly fallen, consolidated). *Albeit* these sites may not be fully representative of the whole Khumbu area, and upper Dudh Koshi catchment, still they provide precious information for snow modeling therein.

3.3. GCM data

Here to simulate future hydrological cycle we fed the hydrological model with properly downscaled meteorological projections from three GCM models. These were taken from the Coupled Model Intercomparison Project, release 5 (CMIP5, Alexander et al., 2013), and are namely ECHAM6 (European Centre HAmburg Model, version 6, Stevens et al., 2013), CCSM4 (Community Climate System Model, version 4, Gent et al., 2011), and EC-Earth (European Consortium Earth system model, version 2.3, Hazeleger et al., 2011). The main features of these three models are reported in Table 2. Climate projections (most notably temperature, and precipitation) are evaluated under three different Representative Concentration Pathways (RCP) scenarios (Moss et al., 2010; IPCC, WG-I, 2013) namely RCP2.6 (optimistic, peak in radiative forcing at 3 W m^{-2} or 490 ppm CO_2 equivalent at 2040, and then decline to 2.6 W m^{-2}), RCP4.5 (cautious, stabilization without overshoot pathway to 4.5 W m^{-2}, or 650 ppm CO_2 eq., at 2070), and RCP8.5 (pessimistic, with rising radiative forcing up to 8.5 W m^{-2}, or 1370 ppm CO_2 eq. by 2100).

4. Methods

4.1. Weather data

We explored the altitudinal variability of temperature and precipitation using monthly meteorological data from EVK2CNR stations, located at different elevations, and available during 2003–2014. We carried exploratory analysis (in Buizza, 2014) of seasonal (pre-monsoon, monsoon, post-monsoon, winter) liquid precipitation from 8 rain gauges (1720–5600 m a.s.l.) in the greater Dudh Koshi catchment. These stations displayed increasing precipitation in all seasons until 3000 m a.s.l. or so, with subsequent decrease until 5600 m a.s.l. Previous similar studies displayed the a negative linear gradient of rainfall above *ca.* 3000 m a.s.l. in the Everest region (Bookhagen and Burbank, 2006; Salerno et al., 2015). Higuchi et al. (1982) found that precipitation along the main valley of the Dudh Koshi river decreases with altitude in the range from 2800 m to 4500 m a.s.l., while Putkonen (2004) found that in the Annapurna precipitation peakes at about 3000 m altitude, and then decreases to the north in the rain shadow of the Himalayan crest. Here, based upon four rainfall stations closest to the catchment (Table 1), and displaying similarly decreasing precipitation, we assumed a vertical dependence of rainfall against elevation as

$$P_y = -0.163 \cdot z + 1132.4, \quad (1)$$

where P_y [mm] is the yearly amount of liquid precipitation, and z altitude in m a.s.l. Our basin, closed at Pheriche, 4258 m a.s.l., is clearly laid above 4000 m a.s.l., and precipitation always decreases with altitude therein. An annual lapse rate is chosen ($R^2 = 0.95$) since seasonal rainfall displayed similar lapse rates against altitude. To build the input rainfall grids, we used Thiessen polygons, and within each polygon the lapse rate in Eq. (1) was applied with respect to the reference station

Table 2
Features of the three adopted GCMs.

Model	Institute	Country	Resolution	Layers	Cells
EC-Earth	Europe-wide consortium	E.U.	1.125° × 1.125°	62	320 × 160
ECHAM6	Max Planck Institute for Meteorology	GER	1.875° × 1.875°	47	192 × 96
CCSM4	National Center for Atmospheric Research	U.S.A.	1.25° × 1.25°	26	288 × 144

Please cite this article as: Soncini, A., et al., Future hydrological regimes and glacier cover in the Everest region: The case study of the upper Dudh Koshi basin, Sci Total Environ (2016), http://dx.doi.org/10.1016/j.scitotenv.2016.05.138

in that polygon, for the sole purpose of estimating precipitation in each cell. Here, Namche Bazar station was not used, given that it is laid outside the catchment. To account for snowfall, we applied a correction to the precipitation input. Daily snowfall at Pyramid AWS was converted into water equivalent using fresh snow density measured at Pyramid during May–June 2014 ($\rho_n = 180$ kg m^{-3}). The so obtained new snow water equivalent volume SWE_n was then added to the daily precipitation series at the Pheriche and Kala Patthar stations, whenever in those stations daily temperature was below freezing. Correction of SWE_n for altitude was also applied using the vertical lapse rate in Eq. (1). Quantitatively, rainfall constitutes the 80%, 77% and 64% of estimated total yearly precipitation at Pheriche, Pyramid and Kala Patthar station, respectively, with snowfall otherwise.

4.2. Debris cover mapping

To create a debris thickness map we relied on a recently developed methodology (see full explanation in *e.g.* Mihalcea et al., 2008a, 2008b) using remote sensing estimates of surface temperature. We used a Landsat 8 scene, close as possible to our field campaign dates (May 22, 2014, 10:26). The thermal Infrared Sensor (TIRS) band 10 was used. Landsat scenes consist of digital numbers DNs, that were converted to temperature (see Coll et al., 2010) by i) DNs conversion into spectral radiance, ii) scene-specific atmospheric correction, and iii) inversion of the Planck function to derive temperature values at each pixel. Our estimated surface temperatures (Buizza, 2014) are consistent with other studies (*e.g.* Casey et al., 2012), both in patterns and absolute values. Then, surface temperature on the glacier was used for debris thickness assessment. We used surface debris temperature together with debris thickness data obtained as reported (Section 3.2, 7 values) to calibrate an exponential function linking debris thickness to surface temperature (similarly to Minora et al., 2015). Subsequently, we used the so obtained equation to estimate debris cover thickness on the Khumbu and Khangri Nup glaciers.

4.3. Ice and snow ablation

Debris cover affects ice melt by altering energy budget of ice (Fujita and Sakai, 2014). In Nepal, debris covered glaciers are on average 15 times larger in area and 5 times longer than clean-ice ones, and constitute 80% of the glaciated area (Fujii and Higuchi, 1977; Fukui et al., 2007). The Khumbu and Khangri glaciers display large debris cover, clearly modulating their response to climate variation (Scherler et al., 2011). Based upon data from our ablation stakes we built a radiation based approach for buried ice melting. By assuming for simplicity a linear gradient of temperature (down to melting point at the debris-ice interface, see explanation of this hypothesis *e.g.* in Kayastha et al., 2000), and by further taking that top debris temperature depends upon both incoming solar radiation, and debris thickness (see *e.g.* Mihalcea et al., 2008a, 2008b for this hypothesis), we developed a simple data driven approach to assess buried ice melt as

$$M_{di} = (1-a_{di})\frac{G_{CSI}}{R_d D_d}, \tag{2}$$

where M_{di} [mm day^{-1}] is melting rate of buried ice, R_d is a thermal resistance factor [W m^{-4} s] to be tuned against observations of ice melt and debris depth as stakes, and γ_{di} is the surface debris albedo. Albedo a_{di} was set here to 0.2, considering the lithology dominating in the study site (see *e.g.* Ragettli et al., 2015). G_{CSI} [W m^{-2}] is the theoretical clear sky, topographically corrected global radiation, reduced (for cloudiness) by way of a clear sky index (*CSI*). *CSI* values were observed for the calibration/validation period, and were randomly extracted from a properly normal distribution calibrated monthly for the future simulations. No visible linkage could be seen between daily *CSI* and precipitation *P*. D_d is the debris depth, or thickness. Eq. (2) is valid until our lowest observed value of $D_d = 0.5$ cm (see Kayastha et al., 2000 that found similar results for $D_d = 0.3$ cm or so). However, average debris cover thickness in our 300 m side cell never reaches below 5 cm or so. Ablation of bare ice and snow was modeled with a mixed (radiation plus temperature) degree-day approach (as done in Pellicciotti et al., 2005), namely

$$\begin{matrix} M_{ci,s} = TMF_{ci,s}(T-T_{th}) + RMF_{ci,s}(1-a_{ci,s})G_{CSI} & if\, T \geq T_{th} \\ M_{ci,s} = 0 & if\, T < T_{th} \end{matrix}. \tag{3}$$

There $M_{ci,s}$ [mm day^{-1}] is the melting of either clean-ice or snow within a cell, $TMF_{ci,s}$ [mm day^{-1} °C^{-1}] and $RMF_{ci,s}$ [mm day^{-1} W^{-1} m^2] are the temperature and radiation melting factors for either clean-ice or snow, $a_{ci,s}$ is the clean ice/snow albedo. Albedo for clean ice was set to 0.4, as from the study of Takeuchi et al. (2000) on the Khumbu glacier. Albedo of snow was set to 0.7, a value obtained using radiation and snow cover data at the Pyramid AWS (Buizza, 2014). T_{th} is an air temperature threshold (0 °C here as from data analysis). Melting factors for bare ice were calculated from our ablation stakes. The snow height (*HS*) data collected at Pyramid during 2003–2014 were used to calibrate (2003–2008) and validate (2009–2014) the snow ablation model.

4.4. Glacio-hydrological modelling

We used here a semi-distributed, cell based hydrological model, developed at Politecnico di Milano. Details of the hydrological components of the model (initially based on altitude belts) are reported in Groppelli et al. (2011a), while the glaciological part (ice ablation, and ice flow) is explained in Soncini et al. (2015). The model tracks the variation of the water content in the ground within one cell *W* [mm] in two consecutive time steps (t, t + Δt), as

$$W^{t+\Delta t} = W^t + R\Delta t + M_s\Delta t + M_i\Delta t - ET\Delta t - Q_g\Delta t. \tag{4}$$

Here using the daily time step *R* [mm day^{-1}] is the liquid rain, M_s [mm day^{-1}] is snowmelt, M_i [mm day^{-1}] is ice melt, *ET* [mm day^{-1}] is actual evapotranspiration, and Q_g [mm day^{-1}] is the groundwater discharge. Overland flow Q_s occurs for saturated soil

$$\begin{matrix} Q_s = W^{t+\Delta t} - W_{Max} & if\, W^{t+\Delta t} > W_{Max} \\ Q_s = 0 & if\, W^{t+\Delta t} \leq W_{Max} \end{matrix}, \tag{5}$$

with W_{Max} [mm] greatest potential soil storage. Potential evapotranspiration is calculated here using Hargreaves equation, requiring temperature data. Groundwater discharge is expressed as a function of soil hydraulic conductivity and water content.

$$Q_g = K\left(\frac{W}{W_{Max}}\right)^k, \tag{6}$$

with *K* [mm day^{-1}] saturated permeability and *k* [.] power exponent. Eqs. (1)–(4) are solved using a semi-distributed cell based scheme (implemented for the first time in Migliavacca et al., 2015), able to depict weather inputs, and subsequent snow and ice cover dynamics at a finer resolution than the previously adopted altitude belt model. Here, we used a module specifically designed to simulate glacier flow (inspired to the model in Wallinga and van de Wal, 1998). We modeled ice flow as driven by a simplified force balance, proportional to shear stress raised to *n*, *i.e.* the exponent of Glen's flow law ($n = 3$, see Oerlemans, 2001; Cuffey and Paterson, 2010, for explanation of Glen's law). When basal shear stress τ_b [Pa] is either known or estimated, and accounting for both deformation and sliding velocity as governed by τ_b, it is possible to model depth averaged ice velocity as

$$V_{ice,\ i} = K_d\tau_{b,i}^n h_{ice,i} + K_s\frac{\tau_{b,i}^n}{h_{ice,i}} \tag{7}$$

with $h_{ice,i}$ [m] ice thickness in the cell *i*, and K_s [m^{-3} year^{-1}] and K_d

[m^{-1} $year^{-1}$] parameters of basal sliding and internal deformation. Model calibration was carried out against observed flow velocities (from our ice stakes) for the Khumbu and Khangri Nup glaciers during 2014. To initialize ice flow model for basin wide simulation, we had to estimate ice thickness $h_{ice,i}$ for each cell (with ice cover). Basal shear τ_b can be taken as

$$\tau_{b,i} = \rho_i g h_{ice,i} \sin\alpha_i, \quad (8)$$

with ρ_i ice density [kg m^{-3}], g gravity acceleration [9.81 m s^{-2}], and α_i local (bedrock) slope. To estimate ice thickness, we set up linearly increasing shear stress up the glacier (with upper bound of 150 kPa, as suggested by Baumann and Stefan Winkler, 2010), and solved Eq. (8) for distributed ice thickness h_{ice}. We used for this purpose a 90 m side grid, *i.e.* with smoothing of ASTER DEM on a 3by3 cell basis (as suggested *e.g.* by Rowan et al., 2015). Smoothing is necessary to avoid inconsistent ice depth assessment as due to superficial ruggedness (*e.g.* ice cliffs, small ponds) of the glaciers, which is not representative of the bedrock slopes. Ice thickness maps were then benchmarked against former ice estimates from radio soundings, gathered during 1999 in seven transects on the Khumbu ablation tongue (see Figs. 6/7 in Gades et al., 2000). Avalanche nourishment on the glaciers is accounted for. When ground slope within a cell is larger than a given threshold, progressively more snow detaches (linearly increasing from 0 to 1 within 30°–60°), and falls in the nearest cell downstream, where it could melt or start transformation into ice (this was first applied by Soncini et al., 2015). Once a year, 10% of snow surviving at the end of the ablation season is shifted into new ice (*i.e.* full ice formation requires 10 years). As an instance, Tandong et al. (1999) investigated ice properties of a Himalayan glacier (Dasoupu glacier) using ice coring, and estimated an ice formation time of *ca.* 14 years.

The flow discharges from each cell are routed to the outlet section through a semi-distributed flow routing algorithm, based on instantaneous unit hydrograph, IUH (Rosso, 1984). The model uses two systems (groundwater, overland) of linear reservoirs in series (n_g and n_s). Each of such reservoirs possesses a time constant (*i.e.*, t_g, t_s), to be tuned against flow data.

4.5. Downscaling of GCM projections

The adopted GCMs overestimate precipitation as observed in the Khumbu Valley (with a Bias factor of to 3 to 6). Therefore, as usually done in hydrological projection exercise precipitation was downscaled. We used an approach based on stochastic space random cascades (SSRCs), which we developed for the purpose (see full account in Bocchiola, 2007; Groppelli et al., 2011b). The downscaling model was tuned for each GCM using the 2003–2014 daily series of precipitation at the P measuring stations as reported in Table 1 (unless for Namche Bazar, outside the basin). The downscaling procedure corrects daily precipitation from the GCM using a random multiplicative process, explicitly considering intermittences (*i.e.*, occurrence of dry spells). A constant term is used to fix average daily bias. A β model (with binomial distribution) generator is used to evaluate the probability that the rain rate for a given day is zero, conditioned upon GCM precipitation being positive (Over and Gupta, 1994). Finally a "strictly positive" generator adds a proper amount of variability to precipitation during spells labeled as wet. The tuned model was used to downscale future precipitation projected by each model under the three RCP scenarios. Temperature downscaling was also carried out, using the 2003–2014 temperature series in 3 stations, as above. A monthly averaged *Delta-T* approach was used to project the temperature values (explained in Groppelli et al., 2011a). Eventually, we obtained series of spatially distributed daily projected precipitation and temperature for each GCM, and each RCP, for a total of 9 scenarios, to be fed to the glacio-hydrological model.

4.6. Glacio-hydrological projections

Glacio-hydrological projections were carried out feeding the hydrological model with the precipitation and temperature scenarios obtained above. We estimated annual, and seasonal average flows until 2100. The potential evolution of glaciers until the end of the century was depicted projecting the amount of ice (volume in m^3) in the basin for every year under each scenario. Moreover, for the purpose of benchmarking, we simulated potential future (until 2100) hydrology and ice cover under a stationary climate, *i.e.* feeding the model with simulated stationary climate series (with statistics of 2003–2014).

5. Results

5.1. Ice and snow ablation

Table 3 reports the results of ice melt model, and Fig. 2 shows scatter plot of estimated ice melt values. For buried ice, model calibration is carried out by fitting the ablation model parameter in Eq. (2), namely R_d against observed data at the stake sites. Validation was then carried out running the glacio-hydrological model, and comparing simulated ablation within cells including stakes, against observed ablation therein. *Albeit* this comparison is possibly inaccurate, given the difference in scale (*i.e.*, use of a 300 × 300 m cell against a point wise value), this exercise quantifies the performance of the model in reproducing distributed buried ice ablation. The Bias (*i.e.*, error on average) in calibration (12 points, see Section 3.2) is −12.9%, with $R^2 = 0.79$, and the value of R_d = 2400 W m^{-4} s. In validation, Bias improves to 6% or so, while R^2 decreases to 0.39. For clean ice ablation a similar procedure is carried out (six ablation values, see Section 3.2), and the two parameters are assessed in Eq. (3), namely $RMF_{ci} = 1.6E^{-2}$ mm day^{-1} W^{-1} m^2, and TMF_{ci} = 2 mm day^{-1} $°C^{-1}$. Bias is −0.6%, and −6% for calibration and validation, and R^2 is 0.8 in both cases. Concerning snow ablation, daily *HS* data at Pyramid were used to calibrate (2003–2008) and validate (2009–2014) the snow ablation model (Fig. 3). We obtained namely $RMF_s = 1E^{-2}$ mm day^{-1} W^{-1} m^2, and TMF_s = 5 mm day^{-1} $°C^{-1}$, with Bias = 5.7/15.3%, and R^2 = 0.87/0.76.

5.2. Debris cover map

Fig. 4a reports debris cover thickness. We found an exponential equation linking debris thickness to surface temperature from Landsat T_{Land} as

$$D_d = 0.03 \exp(0.33 T_{Land}) \quad (9)$$

with $R^2 = 0.70$. Average D_d upon the debris covered area is estimated into $E[D_d] = 0.35$ m. We tentatively investigated the relationship between debris thickness and altitude, also usable for projection of future debris cover (see Soncini et al., 2015). However, no such relationship was found. However debris covered area of the Khumbu glacier spans a vertical extent of 300 m or so from Lobuche to the base camp, making this exercise of little meaning. We decided to hypothesize a constant debris thickness within the current covered area (see Rowan et al., 2015, for modeling of potential debris evolution).

5.3. Ice thickness and ice flow model

Fig. 4b reports ice thickness h_{ice} estimates, while Fig. 4c shows the flow velocities V_{ice}. Average h_{ice} here is of 106 m (total surface area of 62 km^2), with largest values at the Mt. Everest Base Camp (BC, h_{ice} *ca.* 380 m) below Khumbu ice fall. Fig. 5 provides validation of ice flow V_{ice}. Again we report calibration of the ice flow model against point wise measurements (five stakes), and validation against results of the glacio-hydrological model. Bias is −9.9%, and −5.31% respectively, being R^2 0.63, and 0.48, respectively. Average flow velocity as estimated

Please cite this article as: Soncini, A., et al., Future hydrological regimes and glacier cover in the Everest region: The case study of the upper Dudh Koshi basin, Sci Total Environ (2016), http://dx.doi.org/10.1016/j.scitotenv.2016.05.138

Table 3
Glacio-hydrological model parameters, and goodness of fit statistics. **Bold** values are calibrated against observed values.

Parameter	Unit	Description	Value	Method
R_d	[W m^{-4} s]	Thermal resistance factor of debris	**2400**	**Ice stakes ablation**
$a_{di,ci,s}$	[.]	Albedo, buried ice, clean ice, snow	0.2, 0.4, 0.7	Ragettli et al., 2015, Takeuchi et al., 2000, AWS Pyramid
$TMF_{ci,s}$	[mm day^{-1} °C^{-1}]	Thermal melt factor, clean ice, snow	**2**, **5**	**Ice stakes**, **nivometer**
$RMF_{ci,s}$	[mm day^{-1} W^{-1} m^2]	Solar melt factor, clean ice, snow	**1.6E^{-2}**, **1E^{-2}**	**Ice stakes**, **nivometer**
t_g, t_s	[day]	Reservoir time constant, ground/overland	**17**, **2**	**Calibration flows**
n_g, n_s	[.]	Reservoirs, ground/overland	3/3	Rosso, 1984
F_v	[%]	Vegetation cover, average	31	Soil cover
K	[mm day^{-1}]	Saturated conductivity	**2**	**Calibration flows**
k	[.]	Ground flow exponent	**1**	**Calibration flows**
W_{Max}	[mm]	Max soil storage, average	53	Soil cover
θ_w, θ_s	[.]	Water content, wilting, field capacity	0.15, 0.35	Groppelli et al., 2011a
K_s	[m^{-3} y^{-1}]	Ice flow basal sliding coefficient	**9.77E^{-21}**	**Ice stakes velocity**
K_d	[m^{-1} y^{-1}]	Ice flow internal deformation coefficient	**6.63E^{-25}**	**Ice stakes velocity**
$\tau_{b,max}$	[kPa]	Maximum basal shear	150	Baumann and Winkler, 2010
Goodness of fit				
Variable	Unit	Description	Bias (calib/valid)	R^2 (calib/valid)
M_{di}	[mm d^{-1}]	Buried ice ablation	−12.9%/6.04%	0.74/0.39
M_{ci}	[mm d^{-1}]	Clean ice ablation	−0.59%/−5.97%	0.80/0.80
M_s	[mm d^{-1}]	Snow ablation	5.7%/15.3%	0.87/0.76
$V_{ice,i}$	[m y^{-1}]	Ice velocity	−9.90%/−5.31%	0.63/0.48
Q	[m^3 s^{-1}]	Discharge	−4.39%/11.94%	0.93/0.69

here is 17.8 m year^{-1}, with a maximum of 47 m year^{-1} in Khumbu icefall above BC.

5.4. Hydrological model

Fig. 6a reports hydrological model performance during calibration (2012), and validation (2013–2014). In Table 3 the Bias are −4.39%, and 11.9%, respectively, and R^2 of 0.93 and 0.69, respectively. Fig. 6a shows the modeled contribution of each process (*i.e.* ice melt, snow melt, and rainfall plus base flow) to river discharge. Fig. 6b summarizes monthly river discharge and contribution of each flow component. During 2012–2014, flow discharge averages E[Q] = 2.94 m^3 s^{-1}, and the mean ice and snow melt contribution is E[Q_i] = 1.61 m^3 s^{-1}, *i.e.* 55%, and E[Q_s] = 0.57 m^3 s^{-1}, *i.e.* 19%, respectively. Snow melt contributes entirely to discharge (100%) during February to April, where however flow is quite low (0.77 m^3 s^{-1} on average in April). During summer (JJAS) however, the largest share of ice melt is observed (ranging from 55% to 68%, mean 60%). Generally at annual scale, rainfall and base flow amounts to 0.76 m^3 s^{-1}, *i.e.* 26%, while during summer it reaches 28%. Thus ice melt largely drives yearly flows, and especially during monsoon season.

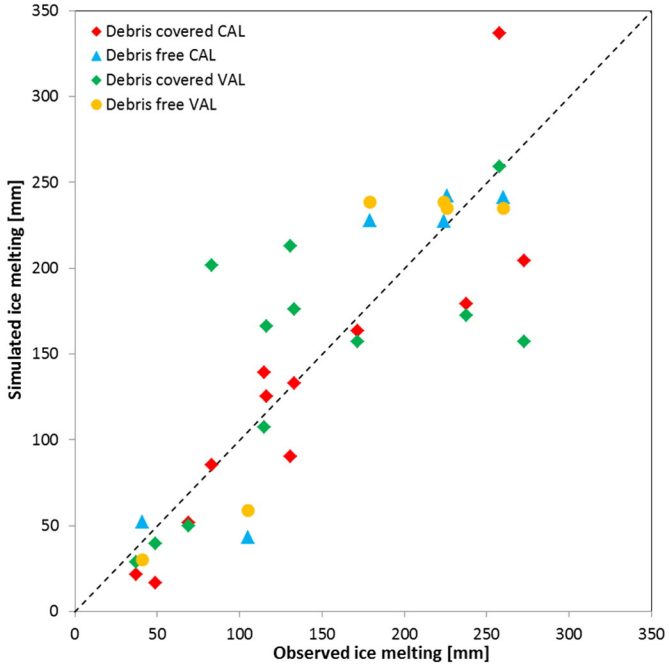

Fig. 2. Ice ablation model. Goodness of fit of the modeled values at stakes. CAL, calibration. VAL, validation.

5.5. Projected climate, hydrology and glaciers' dynamics

Projected climate, in term of precipitation and temperature changes against control period (CR, 2003–2014) is reported in Tables 4 and 5. We consider two reference decades until 2100, namely 2040–2049 (henceforth 2045, or half century), and 2090–2099 (henceforth 2095, or end of century).

Decades are used to be comparable with the CR period 2003–2014. From Table 5 yearly temperature changes consistently between models (*i.e.* all models provide increased temperatures in time, for CR, 2045, and 2095), and RCPs (*i.e.* temperatures are always larger for RCP8.5, than for RCP4.5, and RCP2.6). An exception is given by RCP2.6, where all GCMs consistently provide substantially constant (or even decreasing) temperature between 2045, and 2095. This stems from the nature of RCP2.6, which is an "optimistic" scenario, representative of the literature on mitigation scenarios aiming to limit the increase of global mean temperature to 2 °C (see IPCC, 2013). Visual analysis (not shown for shortness) of temperatures did not display anomalous behavior of temperatures in any of the two chosen decades for any of the three models, and RCPs, so we deem such decades as representative. Similarly holds for precipitation, in spite of its more erratic patterns when compared to temperature.

Fig. 7 report projected monthly hydrological fluxes for the same decades, against simulated values during CR period for discharges, 2012–2014. Furthermore, we report a stationary simulation, carried out in the hypothesis of unchanged climate until 2100, obtained *via* synthetic simulation of stationary climate series (using climate statistics during CR 2003–2014 in Tables 4 and 5).

Figs. 8a,b,c, and 9a,b,c are reported for the same decades as above, and display final ice volume, and average SWE at the end of the accumulation season (October 1), respectively, at different altitudes for each RCP. In Fig. 10a the projected yearly flow until 2100 is given. Also, in

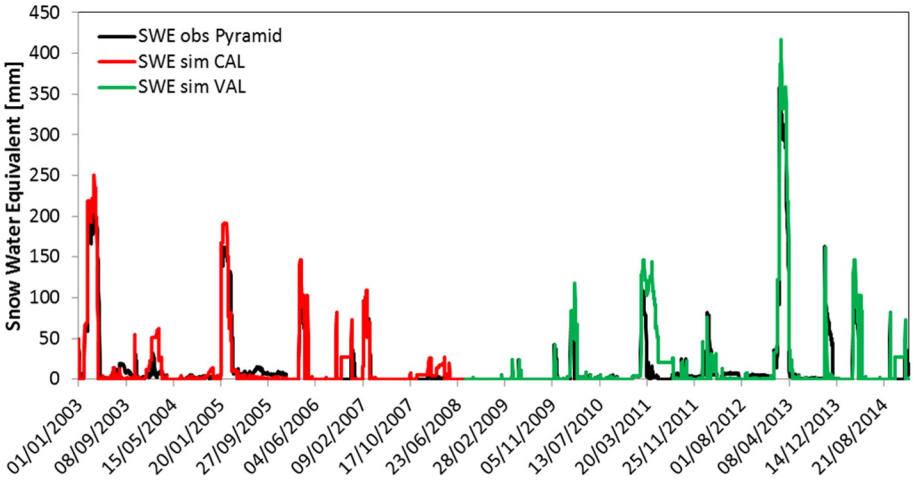

Fig. 3. Snow ablation model, Pyramid snow gauge. CAL, calibration. VAL, validation. Explained in text.

Fig. 10b we report the projected ice volume until 2100, with Fig. 10c reporting projected ice cover area.

Under any model and RCP at half century 2045 an increase of stream flows (Fig. 7) would occur during the warm season, starting from spring (AMJ), with a slight decrease in fall (and in August according to ECHAM6, and CCSM4). The largest increase is seen under RCP8.5, where the largest increase of temperature is expected (Table 5). Notice that according to Table 5, during April in 2045 average basin wide temperature would still be below zero. Conversely, during May temperature would rise close to zero, so providing a tipping point for ice and snow melt. Accordingly, a noticeable increase of melt may occur from May on. However from Fig. 1a, yearly flow would decrease on average at half century (with the exception of EC-Earth for RCP4.5 and RCP8.5, and ECHAM6, for RCP8.5), with an average decrease of −4% against the reference value E[Q] for CR (*i.e.*, 2.94 $m^3\ s^{-1}$).

In 2095, temperature would largely increase in spring especially under RCP8.5. This would result into much earlier melting and seasonal snow depletion (see Fig. 9 displaying available SWE at the end of melt season, October 1), providing large increase of stream flows during April, and even March. However, given the large decrease of ice volume at the lowest altitudes (Fig. 8a,b,c), stream flow would decrease during the melting season. Yearly flow would decrease largely under any scenario, with an average of −26% against E[Q] during CR (Fig. 10a).

Concerning glacier's size, initially ice thinning would occur (so decreasing depth, and volume, Fig. 10b), and then, after ice depletion in a given area, also covered area would decrease (Fig. 10c). Glacier's area may thus be constant, or decrease slowly initially. In Fig. 8 ice volume decreases visibly at 2045, and largely at 2095. In 2045 ice may be thinner than now on average, and yet ice covered area may have changed little (Fig. 10c). At the end of century, given that ice volume would be largely depleted, many cells would become ice-free, and thence the large decrease in ice cover in Fig. 10c. One notices that even under a "stationary" scenario (*i.e.* with climate statistics equivalent to now), ice area and volume would reduce largely after 2030 or so, indicating that the present situation is however unfavorable for glaciers' conservation in the area. Under the warmest scenarios from RCP2.6 to RCP8.5 ice cover would decrease faster than under the stationary scenario, and the most extreme depletion is given by RCP8.5 of ECHAM6 model.

6. Discussion

6.1. Debris cover of Khumbu and Khangri glaciers

Estimated debris cover depth is reported in Fig. Error! Reference source not found. Rowan et al. (2015) investigated debris and ice transport in Khumbu and Khangri Nup glacier during the late Holocene and until 2200. Their simulated present day debris cover map (Fig. 7d therein) has visibly deepest debris cover at the lobes of the ablation tongues, being the upper Khumbu debris free, similarly to our map. Rounce and Mckinney (2014) used i) energy balance, ii) Landsat7 ETM+ imagery, and iii) effective field thermal conductivity, to derive debris thickness in the Everest area, including Khumbu and Khangri. Their debris map (Fig. 7 therein) is qualitatively similar to hours. They report that their results agree relatively well with those by Nakawo et al. (1986), with debris thicker close to the terminal morain, and thinning up the glacier (see also Moribayashi, 1978; Nakawo et al., 1999, indicating similar patterns).

6.2. Snow and ice ablation

Snow ablation was modeled here using *HS* data at Pyramid station during 2003–2014. The use of an enhanced temperature index model is consistent with the available literature (*e.g.* Pellicciotti et al., 2005), and provides reasonable values of the melt factors. Ragettli et al. (2015) for Langtang basin used a hourly (here, daily) enhanced melt factor approach. They found a value of radiation melt factor (for snow and ice) $SRF = 6.25E^{-3}$ mm h^{-1} W^{-1} m^2, compared to $RMF_s = 1.3E^{-3}$ mm h^{-1} W^{-1} m^2 here (hourly melt during 8 h with $T > 0$), and a thermal melt factor (for snow and ice) $TF = 0.18E^{-3}$ mm h^{-1} $°C^{-1}$, against $TMF_s = 0.62$ mm h^{-1} $°C^{-1}$ here (hourly melt during 8 h with $T > 0$). Here, we do not present validation of snow cover using remote sensing data. However we validated snow cover using MODIS data in preliminary studies, with good results (Paramithiotti, 2013; Paramithiotti et al., 2013; Buizza, 2014). Clean ice ablation was also assessed *via* mixed temperature index approach, tuned using ablation stakes. Ragettli et al. (2015) again found $SRF = 6.25E^{-3}$ mm h^{-1} W^{-1} m^2, *vs* our $RMF_s = 2E^{-3}$ mm h^{-1} W^{-1} m^2 (hourly melt during 8 h with $T > 0$). Their thermal melt factor (snow and ice) was $TF = 0.18E^{-3}$ mm h^{-1} $°C^{-1}$, very close to $TMF_s = 0.25$ mm h^{-1} $°C^{-1}$ here (hourly melt during 8 h with $T > 0$). Kayastha et al. (2000) measured ice ablation on Khumbu during 11 days (May 21–June 1, 1999) from a stake farm with different debris cover thickness (0.3 to 40 cm), and on clean ice. On clean ice, they used a thermal melt factor, of 16.9 mm $°C^{-1}$ day^{-1}. Our estimates, covering summer season (May 8–October 9, 2014) provide 24.8 mm $°C^{-1}$ day^{-1}. Kayastha et al. (2000) expressed ice melting rates as per thermal melt factor against debris thickness (see *e.g.* Bocchiola et al., 2010 for an application of this method, and Bocchiola et al., 2015, for a full energy budget model for buried ice ablation). For D_d ranging from 0.3 cm to 10 cm, they found melt factors from 37.2 mm $°C^{-1}$ day^{-1} to 10.1 mm $°C^{-1}$ day^{-1}. During summer 2014 we measured D_d in the range 0.5–9 cm, and we

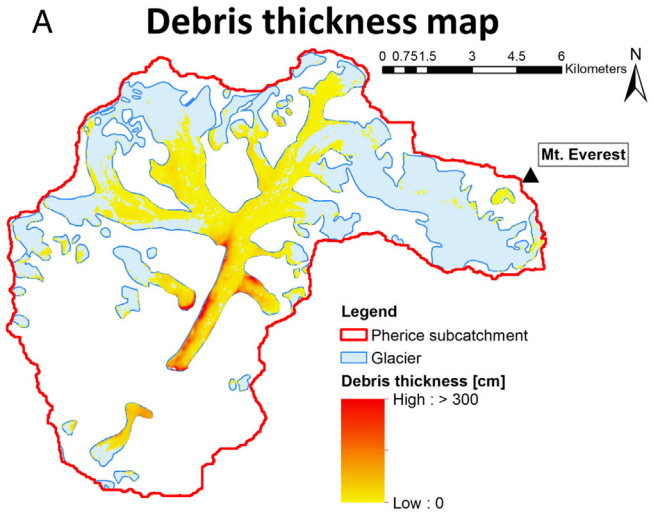

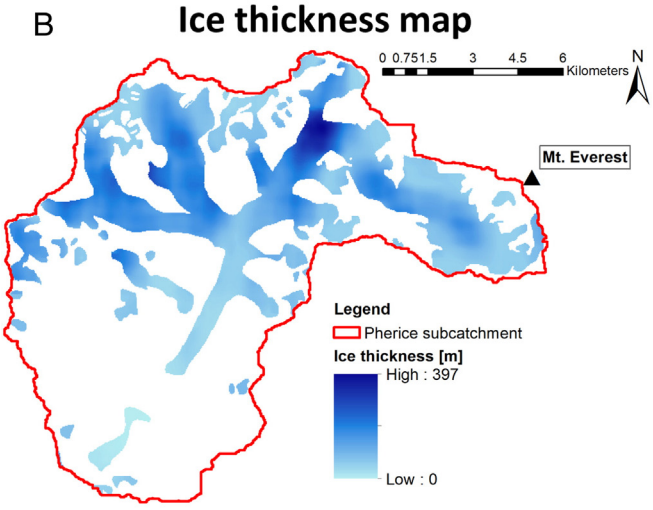

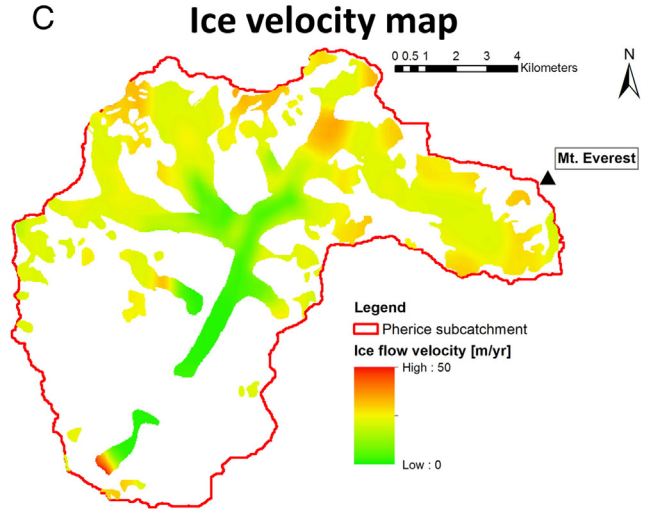

Fig. 4. Spatially distributed maps of debris and ice cover, and velocity. a) Estimated debris cover thickness. b) Estimated ice thickness. c) Estimated flow velocity.

obtained (not shown for shortness) thermal melt factors in the range 21.4–12.3 mm °C^{-1} day^{-1}, with scatter plot well overlapping to that by Kayastha et al. (2000), see Table 1 therein.

While one may stress that few data of ice ablation were available here, still it has to be noticed that few studies so far considered ablation

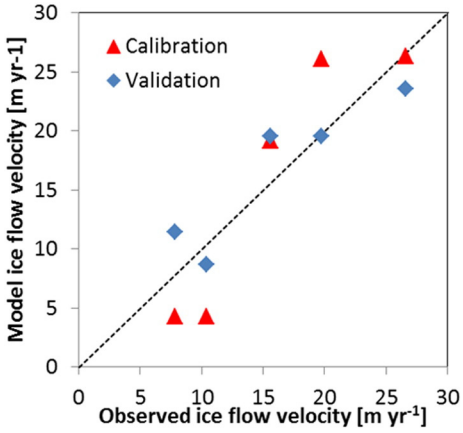

Fig. 5. Ice flow velocity model: goodness of fit of the modeled values at stakes.

on the Khumbu glacier. We do not know if our clean ice ablation is representative for the highest altitudes (*i.e.* above base camp at *ca.* 5500 m a.s.l.), because no measurements of ice ablation were ever take therein. Accordingly, at the moment one may only assume that clean ablation as modeled here is representative also there.

6.3. Ice thickness and ice flow

Ice cover thickness h_{ice} (Reported in Fig. 4b on a 30 m grid) is of large interest, because it drives flow velocity in our model, and provides a condition for long term water resources assessment. Gades et al. (2000) estimated h_{ice} from radio soundings (Figs. 6, and 7 there). They provide h_{ice} of *ca.* 50 m at glacier snout (line L3), subsequently increasing until 170 m or so at Gorak Shep (*i.e.*, where Khangri Nup glacier joins Khumbu, GS line). Subsequently h_{ice} increases until 400 m or so at base camp (BC line). Our map in Fig. 4b displays h_{ice} ranging from 50 m in the low ablation tongue, until a maximum depth of 380 m or so at base camp, with pattern similar to those in Gades et al. (2000). Rowan et al. (2015) estimated present day h_{ice} (Fig. 3 therein). Therein, h_{ice} starts from 50 m or so at the terminus, to increase until 300 m or so at Gorak Shep, and reaching *ca.* 400 m at BC. In the ice fall, h_{ice} decreases rapidly to 150 m or so in the flow line, and is much thinner on the borders. Shea et al. (2015) estimated h_{ice} for some glaciers in the Dudh Koshi area. For Khumbu glacier (Fig. 11d in Shea et al., 2015) they obtained a somewhat high estimated h_{ice} (500 m or so) within the ablation tongue, unlikely according to present literature and local observations. Rowan et al. (2015) modeled present day ice flow velocity V_{ice} (Fig. 8b) using feature tracking for calibration. They obtained a maximum of 150 m year^{-1} or so, in the upper, steeper accumulation zone. Our largest values (Fig. 4c) are close to 50 m year^{-1}, however spatial distribution is consistent. Average V_{ice} in Rowan et al. (2015) was 9 m year^{-1} (and 16 m year^{-1} from feature tracking average) against 12.3 m year^{-1} here (and 15.8 m year^{-1} from the stakes). Quincey et al. (2009) assessed V_{ice} (1992–2002) for some glaciers in the Himalayas, including Khumbu, finding V_{ice} increasing from terminus to BC, from 20 m year^{-1} to 40 m year^{-1} or so (Fig. 3c), very similar to our findings. Similar results were found by Haritashya et al. (2015), displaying somewhat linearly increasing velocity from terminus up the glacier (to BC, Fig. 5 therein), in the range 5 m year^{-1} to 40 m year^{-1}.

6.4. Hydrological model performance and flow components

Flow discharges are available here for few years, and yet such data are precious for modeling hydrology in this high altitude area. As a comparison, Palazzoli et al. (2015) studied Indrawati basin hydrology using daily flow series from two stations, Helambu (2700 m a.s.l., 122 km^2),

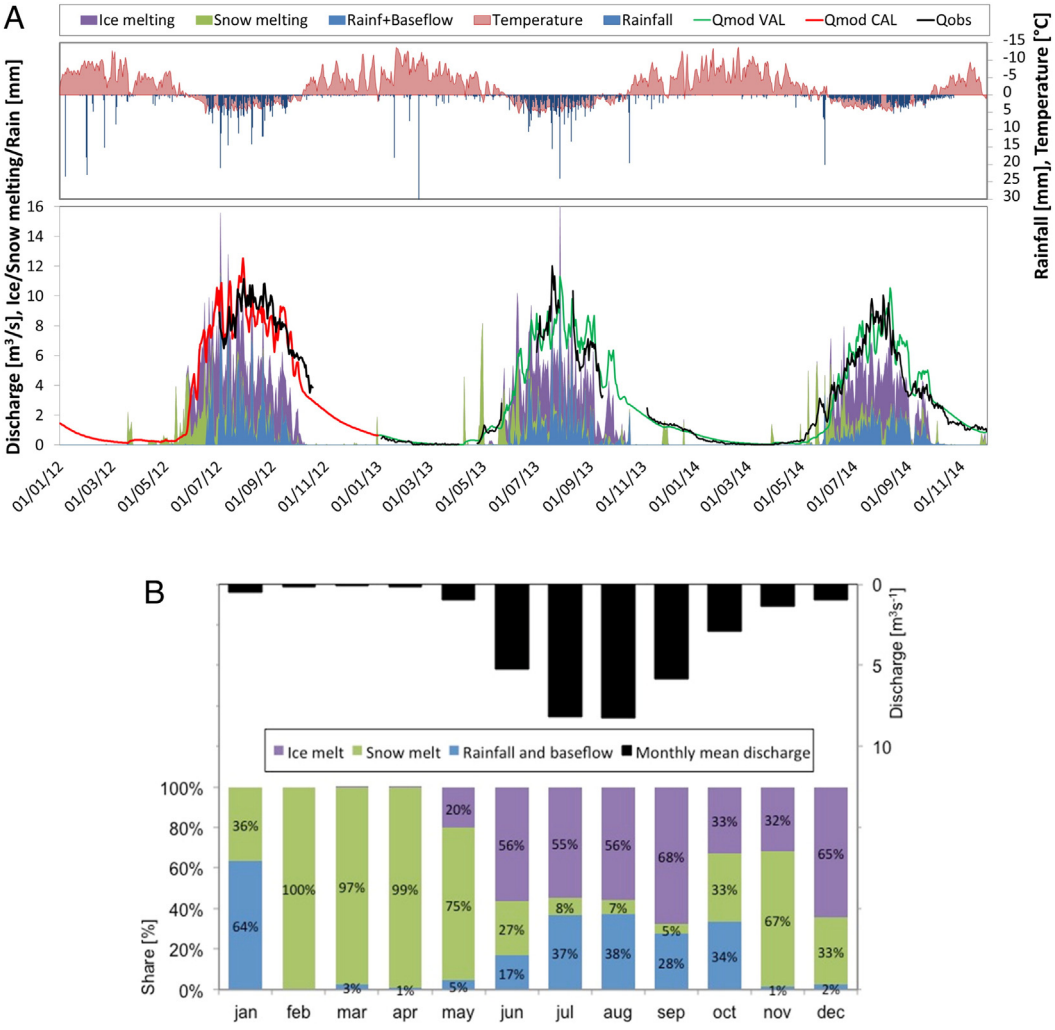

Fig. 6. Hydrological modeling of the Dudh Koshi river closed at Pheriche. a) Daily simulations and observed stream flow. Each flow component is reported (ice melting, snow melting, rainfall and base flow); CAL, calibration. VAL, validation. Temperature and precipitation at Pyramid AWS are also shown (right y axis, values upside down). b) Monthly share of flow components, and mean monthly river discharge (right y axis, values upside down).

and Dolalghat (1050 m a.s.l., 1228 km^2), where 8, and 3 years of data were available, respectively. Ragettli et al. (2015) studied flow components of the upper Langtang basin in Nepal using one year of flow measurements from two stations at the toe of Lirung glacier (*ca.* 3700–4000 m a.s.l.). Savéan et al. (2015) studied water budget of Dudh Koshi river at Rabuwa Bazar (3720 km^2), much downstream Pheriche here, using five years of hydrological data (2001–2005) from Department of Hydrology and Meteorology (DHM) of Nepal.

Table 4
Basin average precipitation changes (%) under our 9 scenarios against control run CR (2003–2014). Monthly and yearly statistics are reported.

Precipitation			Jan	Feb	Mar	Apr	May	Jun	Jul	Aug	Sep	Oct	Nov	Dec	Yearly
CR [mm]			13.9	48.8	12.1	11.0	13.3	40.6	102.7	106.5	44.3	28.1	5.1	2.2	**428.0**
		EC-Earth	−29.9	24.0	−62.1	−33.9	−28.8	21.6	−8.4	12.4	2.2	27.0	44.7	82.6	**4.0**
	RCP2.6	CCSM4	15.5	70.5	−52.7	63.3	−41.3	−10.1	34.7	−20.1	12.8	−36.5	−16.9	59.2	**7.2**
		ECHAM6	115.3	−23.5	71.1	−23.6	12.7	10.0	−8.0	−18.8	43.2	103.3	−41.8	498.8	**10.1**
		EC-Earth	−15.1	3.5	−71.8	−36.1	19.1	9.2	4.0	14.4	6.2	−12.8	18.3	11.5	**3.0**
2040–2049	RCP4.5	CCSM4	45.7	36.1	−39.7	31.4	2.7	−14.0	33.5	−17.3	−29.7	−20.1	13.7	72.2	**2.8**
		ECHAM6	24.5	−73.7	66.2	4.7	3.1	2.8	−2.7	−14.7	28.4	178.9	−13.4	459.9	**7.2**
		EC-Earth	−17.8	18.1	−60.0	30.6	7.7	22.3	−6.1	17.8	9.7	17.0	15.8	26.4	**8.3**
	RCP8.5	CCSM4	17.2	39.3	−9.3	24.0	−9.6	−38.7	21.6	5.2	−24.0	−9.6	60.3	38.6	**4.7**
		ECHAM6	58.9	−41.9	66.5	−50.4	9.5	−20.2	−26.2	−12.3	46.4	164.1	−34.3	466.2	**4.1**
		EC-Earth	−22.5	37.8	−42.0	11.8	−1.3	20.3	−3.5	−10.3	−3.3	−40.2	50.2	100.3	**−1.4**
	RCP2.6	CCSM4	2.4	39.5	−26.7	17.2	8.0	12.9	1.6	−22.6	−60.0	−62.3	3.0	−16.0	**−11.0**
		ECHAM6	92.4	−20.6	100.7	−6.2	−0.1	−1.5	−7.6	−3.9	34.5	215.6	−8.0	579.8	**20.5**
		EC-Earth	−15.7	−4.8	−64.7	1.4	7.0	18.6	12.7	9.2	8.5	67.1	66.8	42.7	**10.9**
2090–2099	RCP4.5	CCSM4	10.6	−10.7	−57.5	1.8	13.0	0.0	27.0	−15.5	−58.3	−38.9	48.1	4.7	**−7.4**
		ECHAM6	−9.1	−67.4	60.3	−25.5	20.1	0.0	−9.0	−12.4	7.2	212.0	−18.6	646.2	**5.8**
		EC-Earth	13.3	−2.2	−64.4	29.1	28.8	21.5	−4.8	28.4	10.9	−0.2	39.8	14.5	**9.7**
	RCP8.5	CCSM4	22.2	46.0	−55.1	80.0	56.7	8.2	17.2	6.2	−45.3	−22.7	62.6	65.8	**8.3**
		ECHAM6	40.1	−33.9	58.6	−21.8	−0.6	−13.5	−13.1	−8.2	45.9	179.7	43.9	399.6	**10.9**

Please cite this article as: Soncini, A., et al., Future hydrological regimes and glacier cover in the Everest region: The case study of the upper Dudh Koshi basin, Sci Total Environ (2016), http://dx.doi.org/10.1016/j.scitotenv.2016.05.138

Table 5
Basin average temperature changes (in °C) under our 9 scenarios against control run CR (2003–2014). Monthly and yearly statistics are reported.

Temperature			Jan	Feb	Mar	Apr	May	Jun	Jul	Aug	Sep	Oct	Nov	Dec	Yearly
	CR [°C]		−9.4	−9.5	−7.5	−5.3	−1.9	1.8	2.8	2.2	0.7	−3.6	−5.3	−6.5	−3.5
		EC-Earth	0.11	0.08	1.00	0.59	0.50	0.29	0.41	0.57	0.69	0.47	0.06	0.05	0.40
	RCP2.6	CCSM4	−0.93	1.29	2.33	1.18	1.38	0.67	0.05	0.23	0.21	−0.85	0.36	−0.31	0.47
		ECHAM6	0.61	0.17	−0.09	0.06	0.39	0.37	1.28	0.71	0.17	0.51	0.49	1.60	0.52
		EC-Earth	0.93	0.62	1.45	1.50	0.85	0.75	0.88	0.81	0.74	0.83	0.85	0.04	0.85
2040–2049	RCP4.5	CCSM4	0.30	1.70	2.77	2.01	2.20	0.66	0.21	0.25	0.80	−0.46	0.04	0.31	0.90
		ECHAM6	0.68	1.29	−0.38	0.36	1.34	1.28	1.66	0.99	0.95	0.95	0.83	1.65	0.97
		EC-Earth	0.84	0.50	1.34	1.31	0.79	1.23	1.28	1.21	1.03	1.43	1.08	0.34	1.03
	RCP8.5	CCSM4	−0.33	2.19	3.11	2.85	1.86	1.18	1.01	0.59	1.07	0.36	0.88	0.96	1.31
		ECHAM6	1.54	1.34	0.28	1.85	2.04	2.25	2.65	1.41	1.20	1.36	0.51	2.45	1.58
		EC-Earth	0.11	0.07	1.33	0.29	0.47	0.18	0.25	0.65	0.27	0.27	0.37	0.27	0.38
	RCP2.6	CCSM4	−0.13	3.00	4.77	3.63	1.56	0.21	0.07	−0.57	−1.88	−2.47	−1.48	−0.93	0.48
		ECHAM6	0.36	1.30	−0.85	−0.03	0.16	0.42	1.24	0.44	0.24	0.10	−0.44	1.06	0.33
		EC-Earth	0.87	0.89	2.73	2.21	1.30	1.44	1.60	1.59	1.34	1.75	1.97	1.31	1.58
2090–2099	RCP4.5	CCSM4	1.08	4.82	5.56	5.53	2.88	1.46	1.05	0.19	−0.58	−1.72	−0.26	0.41	1.70
		ECHAM6	2.28	2.25	1.47	2.83	0.65	1.83	2.31	1.68	1.67	1.23	1.37	2.68	1.86
		EC-Earth	3.02	3.61	5.44	5.03	3.66	3.50	3.80	3.52	3.56	3.87	3.76	3.65	3.87
	RCP8.5	CCSM4	3.84	6.50	7.80	7.50	4.56	3.07	2.62	2.06	1.87	0.93	2.15	2.02	3.74
		ECHAM6	4.96	4.36	2.64	4.28	5.18	5.23	5.08	4.05	3.65	3.72	4.07	5.35	4.38

We highlighted a large contribution of snow and ice melting. Yearly, snow melt contributes for *ca.* 20% of the total flow, with monthly variation up to 100% (Fig. 6b). With an ice cover of 41% of the area, ice melt contributes for 55% of the total flow (Fig. 6b), and during monsoon ice melt contribution reaches 60% or so, with snow melt reaching 12%. Ragettli et al. (2015) estimated for upper Langtang basin (350 km^2,

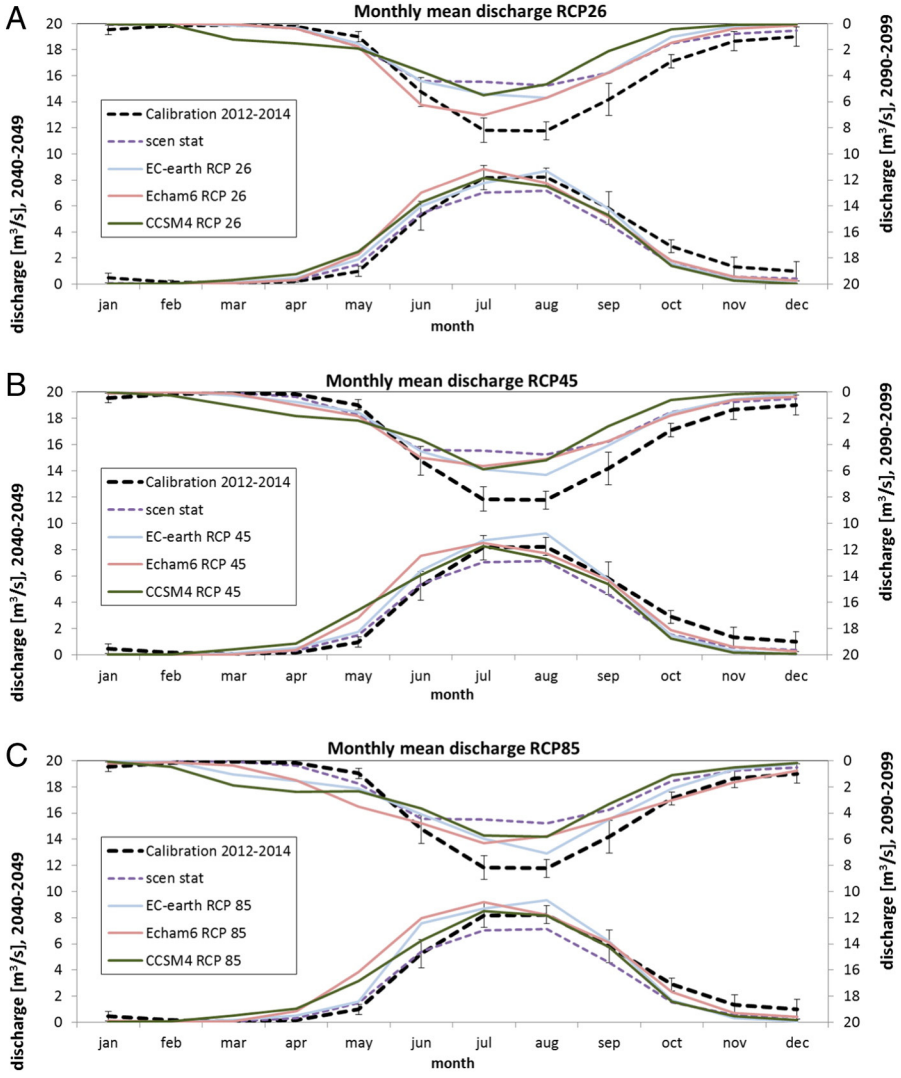

Fig. 7. Hydrological projections of the Dudh Koshi river closed at Pheriche. the monthly river flow is reported as per each GCM model, and stationary scenario, *vs* the calibration period (with confidence limit ±95%). Left y axis, 2040–2049. Right y axis, values upside down, 2090–2099. a) RCP2.6. b) RCP4.5. c) RCP8.5.

Please cite this article as: Soncini, A., et al., Future hydrological regimes and glacier cover in the Everest region: The case study of the upper Dudh Koshi basin, Sci Total Environ (2016), http://dx.doi.org/10.1016/j.scitotenv.2016.05.138

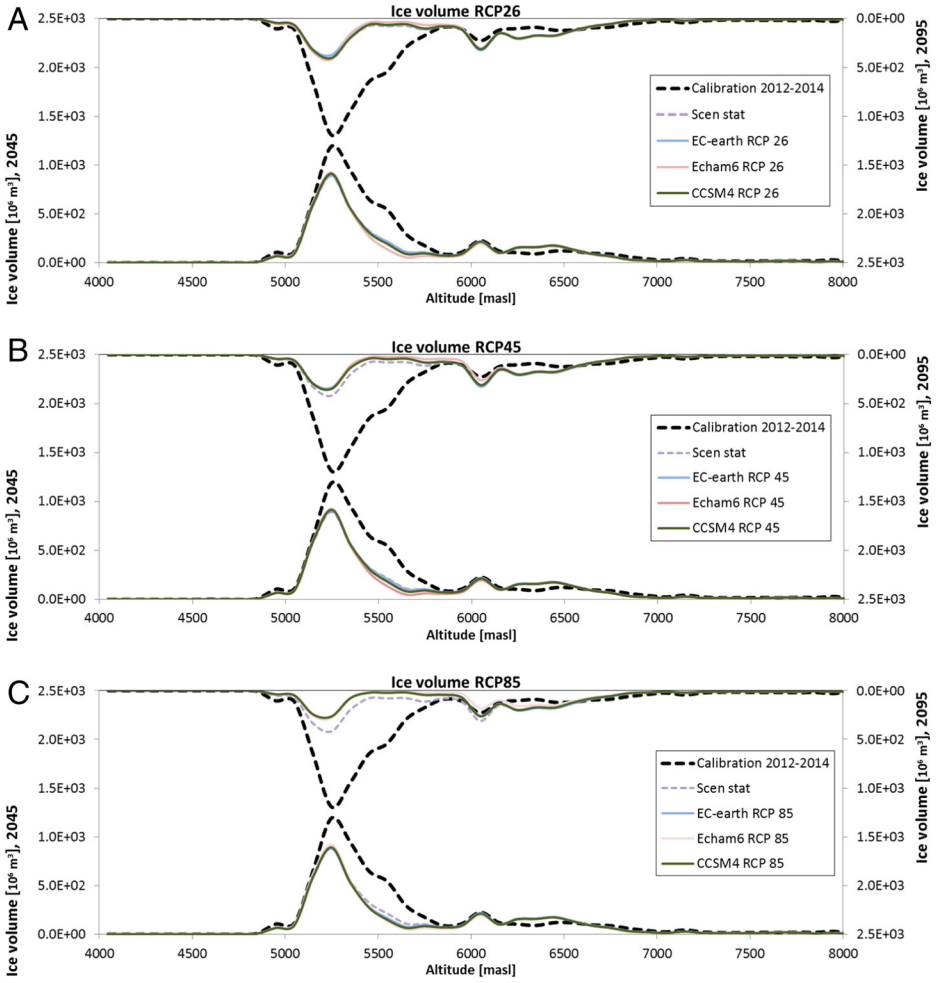

Fig. 8. Glaciological projections for the Khumbu glacier. Ice volume at different elevation belts (100 steps), as per each GCM model, and stationary scenario, *vs* calibration period. Left y axis, 2040–2049. Right y axis, values upside down, 2090–2099. a) RCP2.6. b) RCP4.5. c) RCP8.5.

27% ice cover), a 40% share of snow melt (18% during monsoon), and a 26% of ice melt (and 38% during monsoon), maybe due to smaller ice cover share than here.

6.5. Future climate drivers

Concerning climate change in Nepal, some recent studies are available for benchmark. Among others, Palazzoli et al. (2015) used climate projections for Indrawati river of Nepal from the same GCM models as here. At half century (2045–2054), they found a decadal increase of temperature ranging from +0.6 °C (with RCP2.6 of CCSM4) to +2.3 °C (RCP8.5 of ECHAM6) against 1995–2004, with some variability seasonally (see Table 5). They projected a slight decrease of winter and spring temperature under RCP2.6 of CCSM4. At the end of century (2085–2095) they found increase at the yearly scale ranging from +0.7 °C (RCP2.6 of CCSM4) to +6.2 °C (RCP8.5 of ECHAM6). Shea et al. (2015) studied prospective (until 2100) glaciers' changes in the Everest region, using climate projections from a number of GCM models from the CMIP5 ensemble under RCP4.5, and RCP8.5. They found (Table 5) an average (2021–2050) projected change of temperature from +1.3 (MRI-CGCME, RCP4.5) to +3.1 (ISPL-CM5A-LR, RCP8.5) against reference period 1961–90. Here for the upper Dudh Koshi at 2045 temperature increases from +0.4 °C to +1.6 °C (RCP2.6 of EC-Earth, and RCP8.5 of ECHAM6) against 2003–2014, again with variability seasonally (Table 5). Again here a slight decrease is seen under RCP2.6 (January, October, and December for CCSM4), RCP4.5 (March for ECHAM6), and RCP8.5 (January for CCSM4). At 2095 we found here yearly temperature changes from +0.33 °C (RCP2.6 of ECHAM6) to +4.38 °C (RCP8.5 of ECHAM6), with variability monthly, and some decrease under RCP2.6 and RCP4.5 of CCSM4.

Palazzoli et al. (2015) projected precipitation to change with large variability during the century (Table 5 therein). At 2050 they depicted large potential changes yearly, from +114% (RCP2.6 of CCSM4) to −27% (RCP 8.5 of ECHAM6), and when increase is predicted this largely occurs in fall (OND). At 2090 they projected again some variability, with less oscillation however, from +55% (RCP8.5 of CCSM4) to −18% (RCP4.5 of ECHAM6), with more evenly distributed variation in the season. Shea et al. (2015) provided a range of variation (2021–2050 *vs* 1961–1990) from −3.6% (HADGEM2-CC, RCP8.5) to +16.4% (CANESM2, RCP8.5). Here we projected at 2045 positive variation of *P* at yearly scale, from +3% (EC-Earth, RCP4.5) to +10% (ECHAM6, RCP2.6), with potential for variation seasonally. During the monsoon season, with the largest precipitation here (294 mm, or 68% of yearly precipitation, JJAS), a range of variability is seen from +8.9% (EC-Earth, RCP8.5), to −9.4% (ECHAM6, RCP8.5). At the end of the century, yearly we projected a change from +21% (ECHAM6, RCP2.6) to +11% (EC-Earth, RCP4.5, and ECHAM6, RCP8.5). In the monsoon season we projected a variation from +13% (EC-Earth, RCP8.5) to −14.9% (CCSM4, RCP2.6).

6.6. Future glaciological trends

Ice cover dynamics displayed large potential for glaciers' shrinkage (Fig. 8, 10b,c). From an estimated ice volume of *ca.* 6.27E^9 m^3 (*i.e.*,

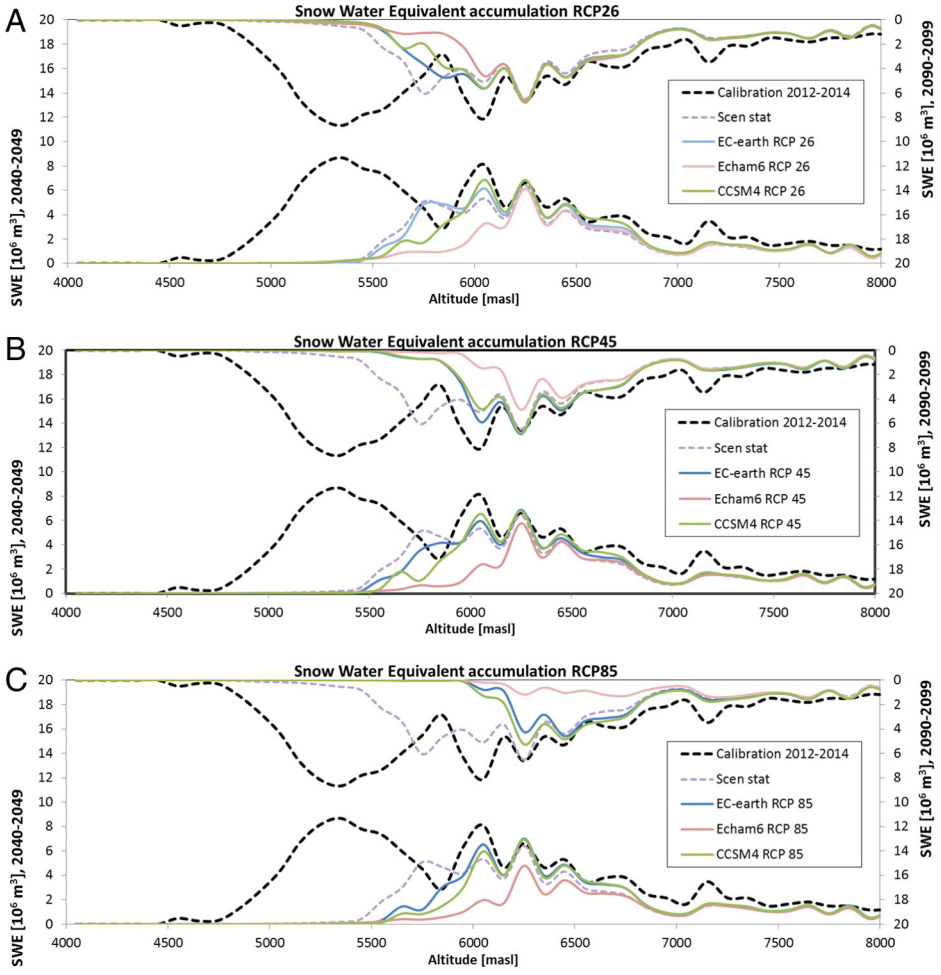

Fig. 9. Glaciological projections for the Khumbu glacier. SWE volume at the end of accumulation season (October 1) at different elevation belts (100 steps), as per each GCM model, and stationary scenario, *vs* calibration period. Left y axis, 2040–2049. Right y axis, values upside down, 2090–2099. a) RCP2.6. b) RCP4.5. c) RCP8.5.

6.27 km^3) in 2010, all of the scenarios, including the stationary one (Scen stat, Fig. 10) provide large ice loss at the end of the century, with a volume ranging from 1.79 km^3 (*i.e.*, −71%, ECHAM6, RCP8.5) to 2.88 km^3 (*i.e.*, −53%, EC-Earth, RCP2.6), and an area from 34.9 km^2 (*i.e.*, −42%, CCSM4, RCP2.6).

As clearly visible comparing Fig. 4a of debris thickness, and Fig. 8, most of ice cover depletion occurs above 5500 m a.s.l. or so, *i.e.*, within the debris free area. At now, the largest volume of ice is in the ablation tongue under debris cover (with a peak in the belt of 5300 m a.s.l. or so). This would be separated from the accumulation zone of the glacier, above 6000 m a.s.l. or so (as seen from loss of ice volume, and subsequent thinning in the range 5500–6000 m a.s.l.). Ice area will therefore shrink (Fig. 10c), however with pockets of sub debris ice in the ablation tongue (Fig. 8, below 5500 m a.s.l.). This has already happened in this area, *e.g.* in the Lobuche glacier, West of Pyramid site (Figs. 1, and 4b). Ice loss would be largely a consequence of lack of snow accumulation at the end of monsoon season. This is clearly visible in Fig. 9, where the amount of SWE available at October 1 in each altitude belt is given. Snow availability under any scenario would be largely decreased, in spite of some scenarios displaying increased precipitation during monsoon, and yearly (Table 4). As a result, even in the presence of a quantifiable increase of monsoonal precipitation, temperature shift will likely offset glaciers' mass balance in the future.

Shea et al. (2015) studied prospective (until 2100) glaciers' changes in the Everest region (Dudh Koshi basin), using climate projections under RCP4.5, and RCP8.5. Considering a set of glaciers covering 32.9 km^3 they projected until 2050 a decrease in volume of −39.3%, and −52.4% on average (between models) for RCP4.5, and 8.5 respectively. Here, these values are −32%, −34%, −35%, and −38%, for Stationary, RCP2.6, RCP4.5, and RCP8.5 scenario respectively. At 2100 they projected changes of −83.7%, and −94.7% on average (between models) for RCP4.5, and 8.5 respectively, *i.e.* substantial disappearance. Here we found at 2100 −53%, −54%, −59%, and −67% for Stationary, RCP2.6, RCP4.5, and RCP8.5 scenario respectively.

Rowan et al. (2015) predicted glacier volume of Khumbu and Khangri Nup glaciers at 2100 and 2200, by imposing a linear rise in ELA of 225 m, to 6225 m (equivalent to warming of +0.9 °C), and of 400 m to 6400 m (equivalent to warming of +1.6 °C) over 100 year, and without a further change in climate until AD2200. They obtained a projected decrease in glacier volume between −8% and −10% (Table 1). Here, a temperature increase nearby 1.5 °C at the end of century roughly points towards the values from RCP4.5 (Table 5). For RCP4.5 in Fig. 10b one projects an ice loss reaching −58% on average, much larger than that projected by Rowan et al. (2015). The proposed comparison mirrors the large degree of uncertainty concerning future glaciological dynamics in the area.

6.7. Future hydrological trends

Hydrological regime of the Dudh Koshi basin was not projected under climate change hitherto that we know of. Our exercise display initially increasing discharges, especially during the monsoon season, and increasing with the RCP (Fig. 7a,b,c). During JJAS present flow averages 6.87 $m^3\ s^{-1}$. At 2045, projected flow varies from 6.75 $m^3\ s^{-1}$ (*i.e.* −2%,

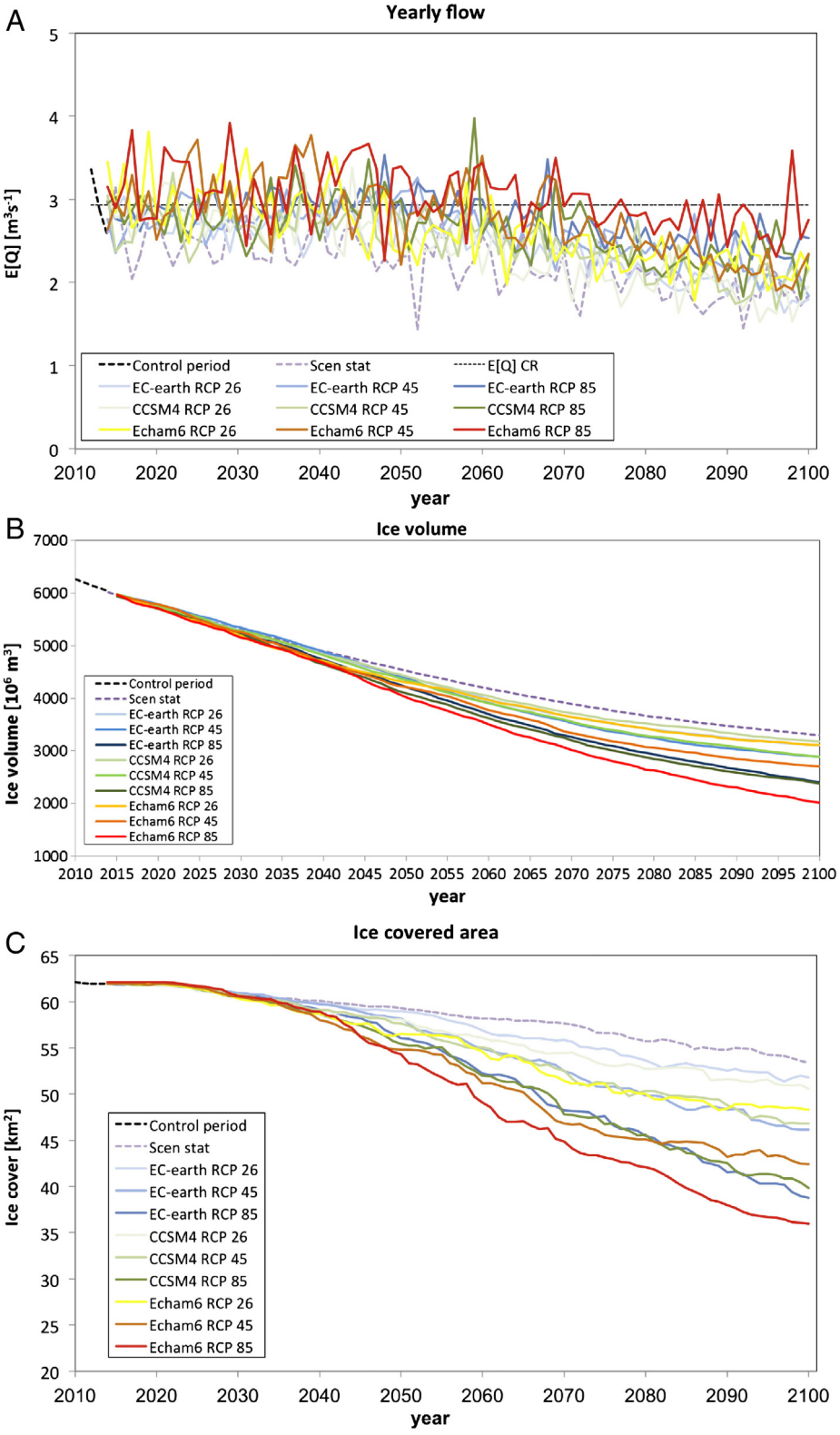

Fig. 10. Hydro-glaciological projections for the Dudh Koshi basin. Yearly flow, ice volume and area as per each GCM model and RCP, and stationary scenario until 2100. a) Flow. b) Ice volume. c) Ice cover area.

CCSM4, RCP4.5) to 7.95 $m^3 s^{-1}$ (*i.e.* +16%, EC-Earth, RCP8.5), averaging 7.3 (*i.e.* +6%). At 2095 however, one has changes from 3.98 $m^3 s^{-1}$ (−42%, CCSM4, RCP2.6) to 5.67 $m^3 s^{-1}$ (−17%, ECHAM6, RCP2.6), averaging 4.93 $m^3 s^{-1}$ (−28%). Seemingly therefore, large glaciers shrinkage during the century may initially increase the available stream flows, but will likely decrease water resources later on, and visibly starting from 2060 or so (Fig. 10a).

Palazzoli et al. (2015) studied projected (until 2100) stream flows within Indrawati basin of Nepal, closed at Dolalghat, displaying no ice cover. At 2050 they found (Fig. 6), an average increase of stream flows

of + 12% during monsoon season, and + 11% at 2090. Excluding however CCSM4 model, depicting very large increase of precipitation (see above), one has − 3%, and − 5% at 2050, and 2090, respectively, as due to joint effect of decreasing precipitation, and increasing evapotranspiration. In this sense, in the Dudh Koshi basin ice cover presence may delay in time flow decrease by buffering water resources until half century. Immerzeel et al. (2013) investigated future ice volume, and runoff from the Langtang basin, Nepal, using outputs of all GCM models from CMIP5 (RCP4.5, RCP8.5). At 2100, in front of a projected decrease of ice volume of − 37%, and − 53% under RCP4.5 and RCP8.5, they found consistently increasing yearly runoff (*vs* 1961–1990) until 2100, from + 31% in 2021–2050 for RCP4.5, to + 88% in 2071–2100 for RCP8.5, that the authors justify with increasing precipitation, and large ice melt.

Our results here seem to indicate some common trends for future hydrological cycle in the Himalayas. Namely, the ongoing and expected future acceleration of ice melt under global warming will initially increase available water in summer. However, in the wake of large ice mass loss, potentially increased precipitation would not be able to offset the negative water balance. The evolution of such situation towards a reduction of available water is visible elsewhere worldwide. For instance in the central Andes largely shrinked ice cover already led to decreasing stream flows, and more decrease is expected for the future (*e.g.* Migliavacca et al., 2015). In the Italian Alps, glaciers' shrinking in the last few decades (Diolaiuti et al., 2012a, 2012b), together with visible decrease of seasonal snow cover (Bocchiola and Diolaiuti, 2010) is likely to have decreased summer flows at the highest altitudes (Bocchiola, 2014). Projections for Alpine catchments indicate reduced summer precipitation, and decreased snowfall during winter, which would be main reason for large prospective reduction of summer stream flows until 2100 (Confortola et al., 2013; Viganò et al., 2015).

Should global warming proceed as depicted from recent modeling exercise, such situation will likely occur also in the Himalayas along the century. Here according to our calculations, at half century yearly contribution of ice melting would be on average (*i.e.* for our 9 scenarios) 45% (*vs* 55% now), and snow melt would increase to 28% (*vs* 19% now). At the end of century ice melt would drop to 31%, and snow contribution would reach 39%. Accordingly, in the future water resources in the upper Dudh Koshi would decrease (by *ca.* − 30% on average in our scenarios), and as well it would depend more largely upon more variable snow melt and rainfall.

Recent findings (Fuss et al., 2014) indicate that recent global temperature evolution substantially overlaps with the projected pattern according to RCP8.5 of IPCC, *i.e.* warming in the last decade proceeded according to the most pessimistic hypothesis. Seemingly therefore, if projections need be made now for the future, globally one may expect that the most credible of our scenarios here are those under RCP8.5.

6.8. Limitations and outlooks

Our modeling exercise has some limitations, also inherent to complex conditions for field studies. Flow data for calibration/validation exercise are available for a short period, which is typical of high altitude basins. The hydrometric station at Periche is still operating, and hopefully it will provide more information for modeling, and testing of our projection exercise.

Our ice ablation model of Khumbu glacier was developed using relatively few stakes on the ground. Use of ice stakes, notwithstanding complex execution in high altitude areas, remains the most accurate method for assessing ice ablation, and the authors carried out several studies worldwide to investigate such facet of glaciers' dynamics (*e.g.* Bocchiola et al., 2010; Soncini et al., 2015; Migliavacca et al., 2015; Minora et al., 2015; Bocchiola et al., 2015). As an instance, Soncini et al. (2015) studied ice ablation upon the 40 km long ablation tongue of the Baltor glacier, Pakistan, deploying 15 ablation stakes, with ablation data gathered during 2011–2013 for most of them. However, Baltoro glacier is at a lower altitude than Khumbu here (from *ca.* 3500 m a.s.l. to *ca.* 4700 m a.s.l., against 5000 m a.s.l. to 5500 m a.s.l. at BC here), and still thick enough to be accessible easily. Also, debris cover is generally thin, unless for the terminus area, and debris can be dug, and studied relatively easily (*e.g.* Mihalcea et al., 2006, 2008b). Khumbu glacier features a noticeable complexity when it comes to field measurements of ice ablation. The high vertical jumps from side morains to glacier surface, given by accelerated glacier shrinking lately, make access to ice difficult for most of its length. Debris cover in the lowest part is very thick, and hardly one can dig into debris in most of the tongue. Deep fractures on the glaciers' surface make it hazardous climbing the ice surface, and fast dynamics and ice collapsing tend to hamper access to stakes, being retrieval quite complicate. In May 2014 we were able to install 3 stakes upon buried ice on the Khangri Nup glacier, but none of those could be found subsequently, likely having collapsed due to snow or debris movement. Two more stakes were installed on the white part of Khangri Nup, but they were not retrieved anymore later. Also one stake on buried ice went lost on the Khumbu, nearby Pyramid site, due to ice collapsing. Ice drilling using Heucke was little efficient as reported, and in our experience use of the drill above 5000 m a.s.l. or so becomes hard for lack of oxygen.

Some glacial lakes are present on Khumbu glacier. On the one side supraglacial lakes make field activity more hazardous, and on the other hand may alter energy budget and ice melting (*e.g.*Benn et al., 2012; Salerno et al., 2012; Thakuri et al., 2015). However, fast dynamics of such lakes, and difficult and hazardous access tracks, makes it difficult to account for such facet, which needs to be considered in the future. Snow melt dynamics was assessed as reported based upon measurements at one only gauge at Pyramid site (Fig. 3), and with some validation using MODIS satellite (500 m resolution, Paramithiotti, 2013; Buizza, 2014), with acceptable results (monthly simulated SWE *vs* monthly mean snow covered area SCA from MODIS, see also Bocchiola et al., 2011), not reported here. In the future, more snow gauges would be necessary for accurate assessment of snow cover in the basin. As a matter of fact debris thickness cover was assessed by calibrating Eq. (9) using few measurements on the ground (in practice 7 values ranging from 0.5–10 cm given Landsat image resolution of 30 m). Distributed sampling of debris thickness was difficult given complex field conditions as reported, especially in the low ablation tongue. Notice however that for deep debris cover (above 10 cm or so in practice) ice ablation tend to reach a somewhat low, rapidly decreasing value in our experiment (see also Kayastha et al., 2000, and Bocchiola et al., 2010; Soncini et al., 2015 for reference on other glaciers). Accordingly, for large debris thickness, a less accurate assessment does not hamper largely ice ablation. Use of constant debris thickness in time may introduce further noise. However here as reported no meaningful relation could be found between D_d and altitude, or slope. In the future, modeling of debris thickness evolution may be of use.

Application of a calibrated model like here for scenario calculations is based on the assumption that the calibration parameters will not change with changing climate. In principle, one could calibrate the model for different periods, and assess model's parameters against climatic and hydrological variables. Given the short available calibration series here this was not possible. Notice that in our model's calibration each parameter is constrained against proper observations (*i.e.* melt factor for snow and ice are constrained against snow/ice), which should provide representative values of the parameters. Model's sensitivity analysis to the calibration parameters, and potential changes of model's parameters against climate may be investigated in the future, say for the hydrological model, when longer available flow data series will be available.

As reported above, large uncertainty is seen concerning future climate trends, and subsequent impact upon glacio-hydrological dynamics. Different RCPs, and models provide substantially increasing temperature, with sign of precipitation change less well defined. For the future it will be important to continue meteorological and

Please cite this article as: Soncini, A., et al., Future hydrological regimes and glacier cover in the Everest region: The case study of the upper Dudh Koshi basin, Sci Total Environ (2016), http://dx.doi.org/10.1016/j.scitotenv.2016.05.138

hydrological monitoring of the area, for the purpose of validating the projected patterns.

7. Conclusions

The response to climate change of the upper Dudh Koshi river, flowing at the toe of the Khumbu glacier in the Everest region, is paradigmatic of potentially changing water resources availability in high altitude, glacier fed basins in the Himalayas. We carried out a thorough investigation of hydrological behavior of the catchment based on new meteorological, glaciological, and hydrological field data, and most recent climate scenarios from CMIP5. We foresee substantially constant stream flows in the future until half century, and a visible decrease thereafter, when ice cover will decrease largely, and hydrological regime will depend more on seasonal snow melting, and monsoonal rainfall, that however increasing will hardly compensate for ice loss. In spite of the large uncertainties, our results provide a relevant benchmark for analysis of future hydrology in the Nepali Himalayas. Water resources are of terrible importance for rural communities in the area, largely relying upon agriculture, and timely assessment of future water availability, and adaptation strategies is paramount necessary. Shrinking glaciers' cover, and increased hazard therein may affect touristic activity, also of large importance for the population of the Khumbu valley, and nearby. Specifically targeted analysis is required to verify whether projected extreme floods and droughts (*i.e.*, maximum and minimum flows for given duration and return period) may considerably worsen until the end of the century. Our study provides a tool that can be used to assess the future hydrological behavior in this high altitude glacierized basins, and in similar ones, useful for policy makers for adaptation purpose.

Acknowledgments

The present work was carried out in fulfillment of SHARE-Paprika, and SHARE RIVER project, funded by the EVK2CNR Association of Italy. We hereby acknowledge the Department of Hydro Meteorology (DHM) of Nepal, for providing weather data from their stations. Nepal Academy of Science and Technology (NAST) is acknowledged for providing personnel and logistic assistance. Mr. Gianpietro Verza, technical coordinator of Pyramid laboratory, and the Pyramid staff are kindly acknowledged for support, and assistance during field campaign and for data gathering. Dr. Chiara Compostella, Dr. Marco Caccianiga, and Dr. Roberto Ambrosini are kindly acknowledged for helping in ice stake survey in fulfillment of their field campaign on Khumbu glacier in 2014. Eng. Vittoria Paramithiotti, and Eng. Michela Buizza are kindly acknowledged for providing help in Dudh Koshi basin modeling in fulfillment of their Master Thesis. We acknowledge the World Climate Research Programme's Working Group on Coupled Modelling, which is responsible for CMIP, and we thank the climate modeling groups (listed in Table 2 of this paper) for producing and making available their model outputs. For CMIP the U.S. Department of Energy's Program for Climate Model Diagnosis and Intercomparison provides coordinating support and led development of software infrastructure in partnership with the “Global Organization for Earth System Science Portals”. Three anonymous reviewers are kindly acknowledged for providing precious suggestions to improve the paper.

References

Aase, T.H., Chaudhary, R.P., Vetaas, O.R., 2009. Farming flexibility and food security under climatic uncertainty: Manang, Nepal Himalaya. Area 42 (2), 228–238. http://dx.doi.org/10.1111/j.1475-4762.2009.00911.x.

Aggarwal, P.K., Joshi, P.K., Ingram, J.S.I., Gupta, R.K., 2004. Adapting food systems of the Indo-Gangetic plains to global environmental change: key information needs to improve policy formulation. Environ. Sci. Pol. 7, 487–498.

Alexander, L.V., et al., 2013. Summary for policymakers. In: Stocker, T.F., et al. (Eds.), Climate Change 2013: The Physical Science Basis. Cambridge University Press, pp. 3–29.

Amatya, L.K., Cuccillato, E., Haack, B., Shadie, P., Sattar, N., Bajracharya, B., Shrestha, B., Caroli, P., Panzeri, D., Basani, M., Schommer, B., Flury, B., Salerno, F., Manfredi, E.C., 2010. Improving communication for management of sociale ecological systems in high mountain areas: development of methodologies and tools d The HKKH Partnership Project. Mt. Res. Dev. 30 (2), 69–79. http://dx.doi.org/10.1659/MRD-JOURNAL-D-09-00084.1.

Barnett, T.P., Adam, J.C., Lettenmaier, D.P., 2005. Potential impacts of a warming climate on water availability in snow-dominated regions. Nature 438 (17), 303–309.

Baumann, S., Stefan Winkler, S., 2010. Parameterization of glacier inventory data from Jotunheimen/Norway in comparison to the European Alps and the Southern Alps of New Zealand. Erdkunde 64, 2,155–2,177.

Beniston, M., 1997. Variations of snow depth and duration in the Swiss Alps over the last 50 years: links to changes in large-scale climatic forcings. Clim. Chang. 36, 281–300.

Benn, D., Bolch, T., Hands, K., Gulley, J., Luckman, A., Nicholson, L., Quincey, D., Thompson, S., Toumi, R., Wiseman, S., 2012. Response of debris-covered glaciers in the Mount Everest region to recent warming, and implications for outburst flood hazards. Earth Sci. Rev. 114 (1), 156–174.

Berthier, E., Arnaud, Y., Kumar, R., Ahmad, S., Wagnon, P., Chevallier, P., 2007. Remote sensing estimates of glacier mass balances in the Himachal Pradesh (Western Himalaya, India). Remote Sens. Environ. 108, 327–338.

Bocchiola, D., 2007. Use of scale recursive estimation for multisensor rainfall assimilation: a case study using data from TRMM (PR and TMI) and NEXRAD. Adv. Water Resour. 30, 2354–2372.

Bocchiola, D., 2014. Long term (1921-2011) changes of Alpine catchments regime in Northern Italy. *Adv. Water Resour.* 70, 51–64.

Bocchiola, D., Diolaiuti, G., 2010. Evidence of climate change within the Adamello Glacier of Italy. Theor. Appl. Climatol. 100 (3-4), 351–369.

Bocchiola, D., Diolaiuti, G., 2013. Recent (1980–2009) evidence of climate change in the upper Karakoram, Pakistan. Theor. Appl. Climatol. 113 (3–4), 611–641.

Bocchiola, D., Rosso, R., 2007. The distribution of daily snow water equivalent in the Central Italian Alps. Adv. Water Resour. 30, 135–147.

Bocchiola, D., Diolaiuti, G., Soncini, A., Mihalcea, C., D'Agata, C., Mayer, C., Lambrecht, A., Rosso, R., Smiraglia, C., 2011. Prediction of future hydrological regimes in poorly gauged high altitude basins: the case study of the upper Indus, Pakistan. Hydrol. Earth Syst. Sci. 15, 2059–2075.

Bocchiola, D., Mihalcea, C., Diolaiuti, G., Mosconi, B., Smiraglia, C., Rosso, R., 2010. Flow prediction in high altitude ungauged basins: a case study in the Italian Alps (Pantano Basin, Adamello Group). Adv. Water Resour. 33, 1224–1234.

Bocchiola, D., Senese, A., Mihalcea, C., Mosconi, B., D'Agata, C., Smiraglia, C., Diolaiuti, G., 2015. An ablation model for debris covered ice: the case study of Venerocolo Glacier (Italian Alps). Geografia Fisica e Dinamica Quaternaria, GFDQ 38 (2), 113–128.

Bolch, T., Kulkarni, A., Kääb, A., Huggel, C., Paul, F., Cogley, J.G., Frey, H., Kargel, J.S., Fujita, K., Scheel, M., Bajracharya, S., Stoffel, M., 2012. The state and fate of Himalayan glaciers. Science 336, 310. http://dx.doi.org/10.1126/science.1215828.

Bolch, T., Pieczonka, T., Benn, D.I., 2011. Multi-decadal mass loss of glaciers in the Everest area (Nepal Himalaya) derived from stereo imagery. Cryosphere 5, 349–358 (Available on line at: http://www.the-cryosphere.net/5/349/2011/tc-5-349-2011.pdf, 2011).

Bookhagen, B., Burbank, D.W., 2006. Topography, relief, and TRMM-derived rainfall variations along the Himalaya. Geophys. Res. Lett. 33, L08405. http://dx.doi.org/10.1029/2006GL026037.

Bookhagen, B., Burbank, D.W., 2010. Towards a complete Himalayan hydrologic budget: the spatiotemporal distribution of snow melt and rainfall and their impact on river discharge. J. Geophys. Res. http://dx.doi.org/10.1029/2009jf001426.

Brown, S., Shrestha, B., 2000. Market-driven land-use dynamics in the middle mountains of Nepal. J. Environ. Manag. 59 (3), 217–225.

Buizza, M., 2014. Hydro-Glaciological Modelling for the Dudh Koshi River Basin, Nepal (Master's thesis) Politecnico di Milano (Available upon request).

Casey, K., Kaab, A., Benn, D., 2012. Geochemical characterization of supraglacial debris via in situ and optical remote sensing methods: a case study in Khumbu Himalaya, Nepal. Cryosphere 6 (1), 85–100.

Chalise, S.R., Kansakar, S.R., Rees, G., Croker, K., Zaidman, M., 2003. Management of water resources and low flow estimation for the Himalayan basins of Nepal. J. Hydrol. 282, 25–35.

Coll, C., Galve, J.M., Sanchez, J.M., Caselles, V., 2010. Validation of Landsat-7/ETM+ thermal-band calibration and atmospheric correction with ground-based measurements. IEEE Trans. Geosci. Remote Sens. 48 (1), 547–555.

Confortola, G., Soncini, A., Bocchiola, D., 2013. Climate change will affect hydrological regimes in the Alps: a case study in Italy. J. Alp. Res. 101 (3). http://dx.doi.org/10.4000/rga.2176.

Cuffey, K.M., Paterson, W.S.B., 2010. The Physics of Glaciers. fourth ed. Academic Press (704 pp., ISBN: 978-0123694614).

Diolaiuti, G., Bocchiola, D., D'agata, C., Smiraglia, C., 2012a. Evidence of climate change impact upon glaciers' recession within the Italian Alps: the case of Lombardy glaciers. Theor. Appl. Climatol. 109 (3–4), 429–445.

Diolaiuti, G., Bocchiola, D., Vagliasindi, M., D'agata, C., Smiraglia, C., 2012b. The 1975–2005 glacier changes in Aosta Valley (Italy) and the relations with climate evolution. Prog. Phys. Geogr. 36 (6), 764–785.

Fujii, Y., Higuchi, K., 1977. Statistical analyses of the forms of the glaciers in the Khumbu Himal: glaciological expedition of Nepal, contribution no. 31. J. Jpn. Assoc. Snow Ice 39, 7–14.

Fujita, K., Sakai, A., 2014. Modelling runoff from a Himalayan debris-covered glacier. Hydrol. Earth Syst. Sci. 18, 2679–2694.

Fukui, K., Fujii, Y., Ageta, Y., Asahi, K., 2007. Changes in the lower limit of mountain permafrost between 1973 and 2004 in the Khumbu Himal, the Nepal Himalayas. Glob. Planet. Chang. 55, 251–256.

Please cite this article as: Soncini, A., et al., Future hydrological regimes and glacier cover in the Everest region: The case study of the upper Dudh Koshi basin, Sci Total Environ (2016), http://dx.doi.org/10.1016/j.scitotenv.2016.05.138

Fuss, S., Canadell, J.G., Peters, G.P., Tavoni, M., Andrew, R.M., Ciais, P., et al., 2014. Betting on negative emissions. Nat. Clim. Chang. 4 (10), 850–853.
Gades, A., Conway, H., Nereson, N., Naito, N., Kadota, T., 2000. Radio Echosounding Through Supraglacial Debris on Lirung and Khumbu Glaciers. IAHS Publication, Nepal Himalayas, pp. 13–24.
Gardelle, J., Berthier, E., Arnaud, Y., 2012. Slight mass gain of Karakoram glaciers in the early twenty-first century. Nat. Geosci. Lett. http://dx.doi.org/10.1038/NGEO1450.
Gent, P.R., Danabasoglu, G., Donner, L.J., Holland, M.M., Hunke, E.C., Jayne, S.R., et al., 2011. The community climate system model version 4. J. Clim. 24, 4973–4991.
Groppelli, B., Bocchiola, D., Rosso, R., 2011a. Spatial downscaling of precipitation from GCMs for climate change projections using random cascades: a case study in Italy. Water Resour. Res. 47, W03519. http://dx.doi.org/10.1029/2010WR009437.
Groppelli, B., Soncini, A., Bocchiola, D., Rosso, R., 2011b. Evaluation of future hydrological cycle under climate change scenarios in a mesoscale Alpine watershed of Italy. Nat. Hazards Earth Syst. Sci. 11, 1769–1785.
Hagg, W., Braun, L., 2005. The influence of glacier retreat on water yield from high mountain areas: comparison of Alps and central Asia. In: De Jong, C., Collins, D., Ranzi, R. (Eds.), Climate and Hydrology of Mountain Areas Vol. 18. Wiley and Sons, England, pp. 263–275.
Hannah, D.M., Kansakar, S.L., Gerrard, A.J., Rees, G., 2005. Flow regimes of Himalayan rivers of Nepal: nature and spatial patterns. J. Hydrol. 308, 18–32.
Haritashya, U.K., Pleasants, M.S., Copland, L., 2015. Assessment of the Evolution in Velocity of Two Debris-Covered Valley Glaciers in Nepal and New Zealand. *Geogr. Ann.: Ser. A, Phys. Geogr.* 97 (4), 737–751.
Hazeleger, W., Wang, X., Severijns, C., Ştefănescu, S., Bintanja, R., Sterl, A., et al., 2011. EC-Earth V2.2: description and validation of a new seamless earth system prediction model. Clim. Dyn. 39, 2611–2629.
Higuchi, K., Ageta, Y., Yasunari, T., Inoue, J., 1982. Characteristics of precipitation during the monsoon season in high-mountain areas of the Nepal Himalaya. Proceed. of the Symposium: Hydrological Aspects of Alpine and High-Mountain Areas Vol. no 138. IAHS Publ., pp. 21–30.
Immerzeel, W.W., Pellicciotti, F., Bierkens, M.F.P., 2013. Rising river flows throughout the twenty-first century in two Himalayan glacierized watersheds. Nat. Geosci. 6 (8), 1–4. http://dx.doi.org/10.1038/ngeo1896.
Immerzeel, W., Petersen, L., Ragettli, S., Pellicciotti, F., 2014. The importance of observed gradients of air temperature and precipitation for modeling runoff from a glacierized watershed in the Nepalese Himalayas. Water Resour. Res. 50 (3), 2212–2226.
Immerzeel, W.W., van Beek, L.P.H., Bierkens, M.F.P., 2010. Climate change will affect the Asian water towers, 328. Nat. Geosci. 5984, 1382–1385. http://dx.doi.org/10.1126/science.1183188.
IPCC, Intergovernmental Panel for Climate Change, 2013. Working Group I Contribution to the IPCC Fifth Assessment Report Climate Change 2013: The Physical Science Basis Summary for Policymakers.
Kääb, A., Berthier, E., Nuth, C., Gardelle, J., Arnaud, Y., 2012. Contrasting patterns of early twenty-first-century glacier mass change in the Himalayas. Nat. Lett. 488, 495–498. http://dx.doi.org/10.1038/nature1132.
Kayastha, R.B., Takehuci, Y., Nakawo, M., Ageta, Y., 2000. Practical prediction of ice melting beneath various thickness of debris cover on Khumbu Glacier, Nepal, using a positive degree-day factor. Debris-Covered Glaciers: Proceedings of an International Workshop Held at the University of Washington in Seattle, Washington, USA, 13–15 September 2000 (264), 71.
Kehrwald, N.M., Thompson, L.G., Tandong, Y., Mosley-Thompson, E., Schotterer, U., Alfimov, V., Beer, J., Eikenberg, J., Davis, M.E., 2008. Mass loss on Himalayan glacier endangers water resources. Geophys. Res. Lett. 35, L22503. http://dx.doi.org/10.1029/2008GL035556.
Konz, M., Uhlenbrook, S., Braun, L., Shrestha, A., Demuth, S., 2007. Implementation of a process-based catchment model in a poorly gauged, highly glacierized Himalayan headwater. Hydrol. Earth Syst. Sci. 11, 1323–1339. http://dx.doi.org/10.5194/hess-11-1323-2007.
Li, P., Shia, C., Li, Z., Mullerd, J.P., Drummond, J., Li, X., Li, T., Li, Y., Li, J., 2012. Evaluation of ASTER GDEM ver2 using GPS measurements, and SRTM ver4.1 in China. ISPRS Annals of the Photogrammetry, Remote Sensing and Spatial Information Sciences, I-4, 181–186, XXII ISPRS Congress, 25 August–01 September 2012, Melbourne, Australia.
Liu, J., Hayakawab, N., Lub, M., Dongc, S., Yuan, J., 2003. Hydrological and geocryological response of winter streamflow to climate warming in Northeast China. Cold Reg. Sci. Technol. 37, 15–24.
Meybeck, M., Green, P., Vorosmarty, C., 2001. New typology for mountains and other relief classes: an application to global continental water resources and population distribution. Mt. Res. Dev. 21, 34–45.
Migliavacca, F., Confortola, G., Soncini, A., Senese, A., Diolaiuti, G., Smiraglia, C., Barcaza, G., Bocchiola, D., 2015. Hydrology and potential climate changes in the Rio Maipo (Chile). Geografia Fisica e Dinamica quaternaria 38, 155–168.
Mihalcea, C., Brock, B.W., Diolaiuti, G., D'Agata, C., Citterio, M., Kirkbride, M.P., Cutler, M.E.J., Smiraglia, C., 2008a. Using ASTER satellite and ground-based surface temperature measurements to derive supraglacial debris cover and thickness patterns on Miage Glacier (Mont Blanc Massif, Italy). Cold Reg. Sci. Technol. 52, 341–354.
Mihalcea, C., Mayer, C., Diolaiuti, G., D'agata, C., Smiraglia, C., Lambrecht, A., Vuillermoz, E., Tartari, G., 2008b. Spatial distribution of debris thickness and melting from remote-sensing and meteorological data, at debris-covered Baltoro glacier, Karakoram, Pakistan. Ann. Glaciol. 48, 49–57.
Mihalcea, C., Mayer, C., Diolaiuti, G., Lambrecht, A., Smiraglia, C., Tartari, G., 2006. Ice ablation and meteorological conditions on the debris covered area of Baltoro Glacier (Karakoram, Pakistan). Ann. Glaciol. 43, 292–300.
Minora, U., Bocchiola, D., D'Agata, C., Maragno, D., Mayer, C., Lambrecht, A., Mosconi, B., Vuillermoz, E., Senese, A., Compostella, C., Smiraglia, C., Diolaiuti, G., 2013. 2001–2010 glacier changes in the Central Karakoram National Park: a contribution to evaluate the magnitude and rate of the Karakoram anomaly. Cryosphere Discuss. (http://www.the-cryosphere-discuss.net/7/2891/2013/tcd-7-2891-2013.html).
Minora, U., Senese, A., Bocchiola, D., Soncini, A., D'agata, C., Ambrosini, R., Mayer, C., Lambrecht, A., Vuillermoz, E., Smiraglia, C., Diolaiuti, G., 2015. A simple model to evaluate ice melt over the ablation area of glaciers in the Central Karakoram National Park, Pakistan. Ann. Glaciol. 56 (70), 202–216.
Moribayashi, S., 1978. Transverse profiles of Khumbu glacier obtained by gravity observation: glaciological expedition of Nepal, contribution no. 46. J. Jpn. Assoc. Snow Ice 40, 21–25.
Moss, R.H., Edmonds, J.A., Hibbard, K.A., Manning, M.R., Rose, S.K., van Vuuren, D.P., Carter, T.R., Emori, S., Kainuma, M., Kram, T., Meehl, G.A., Mitchell, J.F.B., Nakicenovic, N., Riahi, K., Smith, S.J., Stouffer, R.J., Thomson, A.M., Weyant, J.P., Wilbanks, T.J., 2010. The next generation of scenarios for climate change research and assessment. Nature 463, 747–756.
Mukherjee, S., Joshib, P.K., Mukherjeea, S., Ghosh, A., Garg, R.D., Mukhopadhyay, A., 2013. Evaluation of vertical accuracy of open source Digital Elevation Model (DEM). Int. J. Appl. Earth Obs. Geoinf. 21, 205–217.
Nakawo, M., Iwata, S., Watanabe, O., Yoshida, M., 1986. Processes which distribute supraglacial debris on the Khumbu Glacier, Nepal Himalaya. Ann. Glaciol. 8, 129–131.
Nakawo, M., Yabuki, H., Sakai, A., 1999. Characteristics of Khumbu Glacier, Nepal Himalaya: recent change in the debris-covered area. Ann. Glaciol. 28 (1), 118–122.
Nepal, S., Krause, P., Flugel, W., Fink, M., Fischer, C., 2014. Understanding the hydrological system dynamics of a glaciated Alpine basin in the Himalayan region using the J2000 hydrological model. Hydrol. Process. 28 (3), 1329–1344.
Oerlemans, J., 2001. Glaciers and Climate Change (148 pp.) A. A. Balkema Publishers, Brookfield, Vt.
Over, T.M., Gupta, V.K., 1994. Statistical analysis of mesoscale rainfall: dependence of a random cascade generator on large scale forcing. J. Appl. Meteorol. 33, 1526–1542.
Palazzoli, I., Maskey, S., Uhlenbrook, S., Nana, E., Bocchiola, D., 2015. Impact of prospective climate change upon water resources and crop yield in the Indrawati basin, Nepal. Agric. Syst. 133 (C), 143–157.
Paramithiotti, V., 2013. Climate Change Assessment and Hydrological Modelling in the Dudhkosi River Basin, Eastern Nepal (Master's thesis) Politecnico di Milano (Available upon request).
Paramithiotti, V., Bookhagen, B., Soncini, A., Confortola, G., Vuillermoz, E., Diolaiuti, G., Bocchiola, D., 2013. Assessing Hydrologic Components of a Glaciated Basin in the Central Himalaya, Abstract, EGU 2013.
Peel, M.C., Finlayson, B.L., McMahon, T.A., 2007. Updated world map of the Köppen-Geiger climate classification. Hydrol. Earth Syst. Sci. 11, 1633–1644.
Pellicciotti, F., Brock, B., Strasser, U., Burlando, P., Funk, M., Corripio, J., 2005. An enhanced temperature-index glacier melt model including the shortwave radiation balance: development and testing for Haut Glacier d'Arolla, Switzerland. J. Glaciol. 51 (175), 573–587.
Pokharel, S., 2007. Kyoto protocol and Nepal's energy sector. Energ Policy 35, 2514–2525.
Putkonen, J.K., 2004. Continuous snow and rain data at 500 to 4400 m altitude near Annapurna, Nepal, 1999–2001. Arct. Antarct. Alp. Res. 36 (2), 244–248.
Quincey, D., Luckman, A., Benn, D., 2009. Quantification of Everest region glacier velocities between 1992 and 2002, using satellite radar interferometry and feature tracking. J. Glaciol. 55 (192), 596–606.
Ragettli, S., Pellicciotti, F., Immerzeel, W.W., Miles, E.S., Petersen, L., Heynen, M., Shea, J.M., Stumm, D., Joshi, S., Shrestha, A., 2015. Unraveling the hydrology of a Himalayan basin through integration of high resolution in situ data and remote sensing with an advanced simulation model. Adv. Water Resour. 78, 94–111.
Rees, H.G., Holmes, M.G.R., Fry, M.J., Young, A.R., Pitson, D.G., Kansakar, S.R., 2006. An integrated water resource management tool for the Himalayan region. Environ. Model. Softw. 21, 1001–1012.
Rohrer, M.B., Braun, L.N., Lang, H., 1994. Long term records of snow cover water equivalent in the Swiss Alps: 1. Analysis. Nord. Hydrol. 25, 53–64.
Rosso, R., 1984. Nash model relation to Horton order ratios. Water Resour. Res. 20 (7), 914–920.
Rounce, D., McKinney, D., 2014. Debris thickness of glaciers in the Everest area (Nepal Himalaya) derived from satellite imagery using a nonlinear energy balance model. Cryosphere 8 (4), 1317–1329.
Rowan, A.V., Egholm, D.L., Quincey, D.J., Glasser, N.F., 2015. Modelling the feedbacks between mass balance, ice flow and debris transport to predict the response to climate change of debris-covered glaciers in the Himalaya. Earth Planet. Sci. Lett. 430, 427–438.
Salerno, F., Buraschi, E., Bruccoleri, G., Tartari, G., Smiraglia, C., 2008. Glacier surface-area changes in Sagarmatha National Park, Nepal, in the second half of the 20th century, by comparison of historical maps. J. Glaciol. 54 (187), 738–752.
Salerno, F., Guyennon, N., Thakuri, S., Viviano, G., Romano, E., Vuillermoz, E., Cristofanelli, P., Stocchi, P., Agrillo, G., Ma, Y., Tartari, G., 2015. Weak precipitation, warm winters and springs impact glaciers of south slopes of Mt. Everest (central Himalaya) in the last 2 decades (1994–2013). Cryosphere 9 (3), 1229–1247.
Salerno, F., Thakuri, S., D'Agata, C., Smiraglia, C., Mnfreid, E.C., Viviano, G., Tartari, G., 2012. Glacial lake distribution in the Mount Everest region: uncertainty of measurement and conditions of formation. Glob. Planet. Chang. 92–93, 30–39.
Salerno, F., Viviano, G., Mangredi, E.C., Caroli, P., Thakuri, S., Tartari, G., 2013. Multiple carrying capacities from a management-oriented perspective to operationalize sustainable tourism in protected area. J. Environ. Manag. 128, 116–125. http://dx.doi.org/10.1016/j.jenvman.2013.04.043.
Savéan, M., Delclaux, F., Chevallier, P., Wagnon, P., Gonga-Saholiariliva, N., Sharma, R., Neppel, L., Arnaud, Y., 2015. Water budget on the Dudh Koshi River (Nepal): uncertainties on precipitation. J. Hydrol. 531, 850–862.
Scherler, D., Bookhagen, B., Strecker, M.R., 2011. Spatially variable response of Himalayan glaciers to climate change affected by debris cover. Nat. Geosci. 4 (3), 156–159.

Please cite this article as: Soncini, A., et al., Future hydrological regimes and glacier cover in the Everest region: The case study of the upper Dudh Koshi basin, Sci Total Environ (2016), http://dx.doi.org/10.1016/j.scitotenv.2016.05.138

Sharma, C.K., 1996. Overview of Nepal's energy sources and environment. Atmos. Environ. 30 (15), 2717–2720.
Shea, J.M., Immerzeel, W.W., Wagnon, P., Vincent, C., Bajracharya, S., 2015. Modelling glacier change in the Everest region, Nepal Himalaya. Cryosphere 9, 1105–1128. http://dx.doi.org/10.5194/tc-9-1105-2015.
Soncini, A., Bocchiola, D., Confortola, G., Bianchi, A., Rosso, R., Mayer, C., Lambrecht, A., Palazzi, E., Smiraglia, C., Diolaiuti, G., 2015. Future hydrological regimes in the upper Indus basin: a case study from a high-altitude glacierized catchment. J. Hydrometeorol. 16, 306–326.
Stevens, B., Giorgetta, M., Esch, M., Mauritsen, T., Crueger, T., Rast, S., et al., 2013. Atmospheric component of the MPI-M earth system model: ECHAM6. J. Adv. Model. Earth Syst. 5, 1–27.
Tadono, T., Takaku, J., Shimada, M., 2012. Validation study on ALOS prism DSM mosaic and ASTER GDEM 2. ISPRS Annals of the Photogrammetry, Remote Sensing and Spatial Information Sciences, I-4, 193–198. XXII ISPRS Congress, 25 August–01 September 2012, Melbourne, Australia.
Takeuchi, Y., Kayastha, R.B., Nakawo, M., 2000. Characteristics of ablation and heat balance in debris free, and debris covered areas of Khumbu glacier, Nepal Himalayas, in the pre-monsoon season. Proceedings of the Workshop: Debris Covered Glaciers, Seattle, Washington, USA, September 2000. IAHS, 264, pp. 53–61.
Tandong, Y., Jianchen, P., Ninlian, W., Lide, T., 1999. A new type of ice formation zone found in the Himalayas. Chin. Sci. Bull. 44 (5), 469–474.
Tartari, G., Salerno, F., Buraschi, E., Bruccoleri, G., Smiraglia, C., 2008. Lake surface area variations in the north-eastern sector of Sagarmatha National Park (Nepal) at the end of the 20th Century by comparison of historical maps. J. Limnol. 67, 139–154.
Thakuri, S., Salerno, F., Bolch, T., Guyennon, N., Tartari, G., 2015. Factors controlling the accelerated expansion of Imja Lake, Mount Everest region, Nepal. Ann. Glaciol. 57, 245–257. http://dx.doi.org/10.3189/2016AoG71A063.
Thakuri, S., Salerno, F., Smiraglia, C., Bolch, T., D'Agata, C., Viviano, G., Tartari, G., 2014. Tracing glacier changes since the 1960s on the south slope of Mt. Everest (central Southern Himalaya) using optical satellite imagery. Cryosphere 8, 1297–1315.
Viganò, G., Confortola, G., Fornaroli, R., Canobbio, S., Mezzanotte, V., Bocchiola, D., 2015. Future climate change may affect habitat in Alpine streams: a case study in Italy. ASCE J. Hydrol. Eng. 21 (2). http://dx.doi.org/10.1061/(ASCE)HE.1943-5584.0001293.
Viviroli, D., Dürr, H.H., Messerli, B., Meybeck, M., Weingartner, R., 2007. Mountains of the world, water towers for humanity: typology, mapping, and global significance. Water Resour. Res. 43, W07447. http://dx.doi.org/10.1029/2006WR005653.
Wallinga, J., van de Wal, R.S.W., 1998. Sensitivity of Rhonegletscher, Switzerland, to climate change: experiments with a one-dimensional flowline model. J. Glaciol. 44 (147), 383–393.
Yao, T., Thompson, L., Yang, W., Yu, W., Gao, Y., Guo, X., Yang, X., Duan, K., Zhao, H., Xu, B., Pu, J., Lu, A., Xiang, Y., Kattel, D.B., Joswiak, D., 2012. Different glacier status with atmospheric circulations in Tibetan Plateau and surroundings. Nat. Clim. Chang. 2, 663–667. http://dx.doi.org/10.1038/nclimate1580.
Zemp, M., Hoelzle, M., Haeberli, W., 2009. Six decades of glacier mass-balance observations: a review of the worldwide monitoring network. *Ann. Glaciol.* 50, 101–111.

Please cite this article as: Soncini, A., et al., Future hydrological regimes and glacier cover in the Everest region: The case study of the upper Dudh Koshi basin, Sci Total Environ (2016), http://dx.doi.org/10.1016/j.scitotenv.2016.05.138